SOME SELF-CONSISTENT TWO-STATE SLIDING FILAMENT MODELS OF MUSCLE CONTRACTION

TERRELL L. HILL, EVAN EISENBERG, YI-DER CHEN, *and* R. J. PODOLSKY

From the Laboratory of Molecular Biology, National Institute of Arthritis, Metabolism, and Digestive Diseases, the Laboratory of Biochemistry, National Heart and Lung Institute, and the Laboratory of Physical Biology, National Institute of Arthritis, Metabolism, and Digestive Diseases, National Institutes of Health, Bethesda, Maryland 20014

ABSTRACT The general formalism required to treat two-state sliding filament models of muscle contraction, including free energy considerations, is first reviewed and amplified. This formalism is then used to examine, and modify as needed, three models studied previously by Podolsky and Nolan, in which cross-bridge attachment-detachment and ATP turnover are not tightly coupled. No attempt is made here to establish an optimal, self-consistent model of this type because our interest is primarily in methodology rather than in fitting experimental results. But it appears from this preliminary study that such a model, with satisfactory mechanical and thermodynamic properties, could be found. An extremely simple but unrealistic two-state model is also studied which is of interest because it demonstrates the fact that it is possible, in principle at least, for sliding filament models to work with very high thermodynamic efficiencies (50–100%). An appendix is included that is concerned with the form of the dependence of certain first-order rate constants on the concentrations of ATP, ADP, and P.

1. INTRODUCTION

The sliding filament model is currently much used as a working hypothesis for the molecular mechanism of contraction of vertebrate striated muscle. Implicit in the sliding filament hypothesis, though not widely realized, is a general theoretical formalism (Hill, 1968*a*, 1974, 1975*a*) that involves an appropriate combination of thermodynamics, statistical mechanics, and biochemical kinetics. This paper is the third of a series that is intended to illustrate the proper application of this general formalism to particular models.

In the first two papers (Chen and Hill, 1974; Hill and Chen, 1974) a very simple, prototypal, two-state model was used for the purpose of explicit examination of fundamental theoretical questions such as behavior of the model near equilibrium as well as far from equilibrium, the Onsager reciprocal relation, thermodynamic efficiency of ATP free energy conversion, entropy production, etc. This particular model was chosen for convenience only and was not meant to be a practical or realistic model of muscle contraction.

The present paper is also limited to two-state models (one kinetically significant attached state; one kinetically significant unattached state). But our primary objective here (section 4) is to start with some of the models, with realistic mechanical properties, previously studied by Podolsky and Nolan (1971, 1973) and to investigate the modifications of these models that are required in order to render them complete and self-consistent in accordance with the general theoretical formalism mentioned above. Similar modifications are presumably required in most previously published explicit models of the sliding filament type.

We supplement section 4 with: essential free energy considerations for two-state models (section 2); a summary of some of the fundamentals of the formalism, as applied to two-state models (section 3); an analysis of an idealized two-state model designed to show that it is possible in principle to obtain very high efficiencies in a sliding filament system (section 5); and an appendix on the dependence of certain rate constants of the formalism on the concentrations of ATP and products (ADP, P). Small print is used for certain material that is not necessary to the main argument.

We are presently investigating models with more than two biochemical states and with multiple actin sites (Hill, 1973; Hill, 1975*a*, section IV). It is our intention in these models to use current biochemical and structural knowledge as an important guide in the selection of states and parameters. The models in section 4 of the present paper were constructed (Podolsky and Nolan, 1973) to fit mechanical data primarily, especially isotonic transients.

2. FREE ENERGY CONSIDERATIONS FOR TWO-STATE MODELS

Our main object here and in section 3 is to summarize theoretical principles that are essential for an understanding of sections 4 and 5. In addition, sections 2 and 3 should be of value for some readers as a relatively simple, though condensed, introduction to the two long and much more general papers available on this subject (Hill 1974, 1975*a*). It is assumed that the reader is acquainted with structural and other features of the sliding filament model of muscle contraction (H. E. Huxley, 1969; Carlson and Wilkie, 1974).

We consider an ensemble of independent and equivalent cross-bridges in the overlap zone, each of which has accessible to it at most one actin attachment site at a time. We use the term "cross-bridge" to apply to a projection from a myosin filament whether it is attached to an actin site or not. A cross-bridge can exist in various biochemical states, as illustrated in Fig. 1, where M = myosin cross-bridge, A = actin site, T = ATP, and D = ADP, P (treated as a single entity for simplicity). Fig. 1 is called a "diagram." Each line represents a pair of possible inverse first-order transitions. The heavy lines indicate what is currently presumed to be the dominant cycle (involving five states). For simplicity and concreteness, only this cycle is considered below. The net flux around this cycle is in the counterclockwise direction (resulting in $T \rightarrow D$).

Actually, such a cycle must be considered at each value of a structural variable x. But this complication is not an essential feature here, and is therefore reserved for the

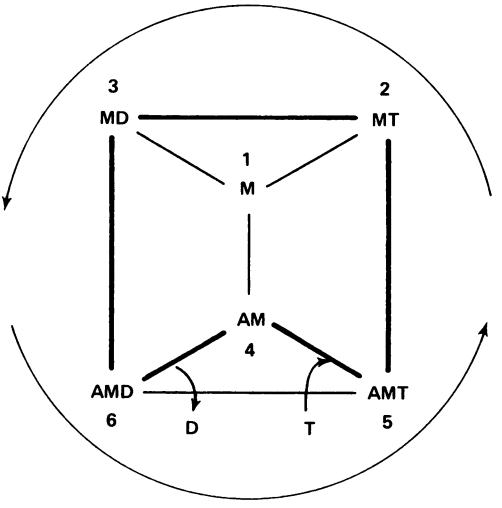

FIGURE 1 Six-state diagram for a myosin cross-bridge. Each line represents both forward and backward first-order transitions. See text for further details.

next section. With x dependence excluded, the treatment in the present section is in fact applicable as well to other biochemical systems that employ ATP as a free energy source, e.g., active transport (Hill, 1968*b*, Chapter 7; Hill, 1975*b*). In active transport, we are concerned with an ensemble of independent and equivalent transport units or channels (rather than cross-bridges).

In this section, we first summarize the assumptions of the formalism. Using the five-state cycle in Fig. 1 as an example, we then discuss the relations between free energy levels and rate constants in this cycle. Finally, we examine the same relations for two-state cycles obtained by "reduction" (Hill, 1975*a*, Appendix 2) of the original cycle. That is, because some of the original rate constants are (by assumption) large compared with others, we consider that the number of *effective* or necessary states can be reduced from five to two.

(a) Summary of Assumptions

A thorough discussion of the assumptions of the formalism has been published (Hill, 1974). However, we give a very brief summary of these assumptions, as applicable here, as an aid to the reader. They are as follows (some have been mentioned above). (*a*) At any instant a given cross-bridge has accessible to it, for attachment with significant probability, only a *single* actin site. (*b*) The cross-bridge behaves operationally as if it has only one head. (*c*) The ATP hydrolysis products ADP+P can be treated as a single species. (*d*) Cross-bridges in the overlap zone act independently of each other. (*e*) The kinetic and mechanical behavior of a cross-bridge is independent of the myosin-actin interfilament spacing. (*f*) A cross-bridge can exist in several different discrete biochemical states (providing the diagram), some attached to actin and some

unattached, and transitions between these states include the binding and splitting of ATP.

Implicit in (*f*) are the following: the states of the diagram are in general not in equilibrium *with each other,* yet each state is an equilibrium state *internally;* transitions between states occur "instantaneously" (on the time scale of the diagram); force exerted by a cross-bridge on an actin filament is associated with *attached states* and *not with transitions;* a nonzero force per cross-bridge (under nonequilibrium conditions) is a consequence of the effect of myofilament structural asymmetry on the rate constants of the diagram and possibly on the forces associated with attached states; and the molecular rate constants of the diagram (for any given model) are oblivious of (i.e. invariant to) the kind of experiment being conducted and hence do not depend at all on the macroscopic load or on the velocity of contraction.

Actually, the above assumptions and their consequences are not new, aside from having been set out explicitly and in detail (Hill, 1974). They are *implicit* [except for (*c*)] in the earlier work of A. F. Huxley (1957), Hill (1968*a*), Podolsky et al. (1969), Podolsky and Nolan (1971, 1973), and others.

(b) Five-State Cycle

To simplify notation, we number the states as shown in Fig. 1. Let α_{ij} be the first-order rate constant for the transition $i \rightarrow j$. As demonstrated with the aid of detailed balance in Hill (1974, pp. 278 and 325–327), equilibrium constants, *defined* as rate constant ratios, are related to free energy differences in successive counterclockwise steps around the cycle, as follows:

$$K_{45} \equiv \alpha_{45}/\alpha_{54} = \exp[-(A_5 - A_4 - \mu_T)/kT] \tag{1}$$

$$K_{52} \equiv \alpha_{52}/\alpha_{25} = \exp[-(A_2 - A_5)/kT] \tag{2}$$

$$K_{23} \equiv \alpha_{23}/\alpha_{32} = \exp[-(A_3 - A_2)/kT] \tag{3}$$

$$K_{36} \equiv \alpha_{36}/\alpha_{63} = \exp[-(A_6 - A_3)/kT] \tag{4}$$

$$K_{64} \equiv \alpha_{64}/\alpha_{46} = \exp[-(A_4 - A_6 + \mu_D)/kT]. \tag{5}$$

In these equations, A_i is the Helmholtz free energy of the cross-bridge in state i (the Gibbs free energy differs by a negligible pV_i term), while the chemical potentials μ_T and μ_D are related to concentrations (omitting activity coefficients for simplicity) in the usual way by

$$\begin{aligned} \mu_T &= \mu_T^0 + kTln\, c_T \\ \mu_D &= \mu_D^0 + kTln\, c_D. \end{aligned} \tag{6}$$

Here $c_D = c_{ADP}$ or c_P, assuming (for simplicity) only one of these is varied in a given set of experiments. The free energy A_i refers to a *single* independent cross-bridge (a "small" thermodynamic system) fixed in the myofilament structure. Thus A_i has

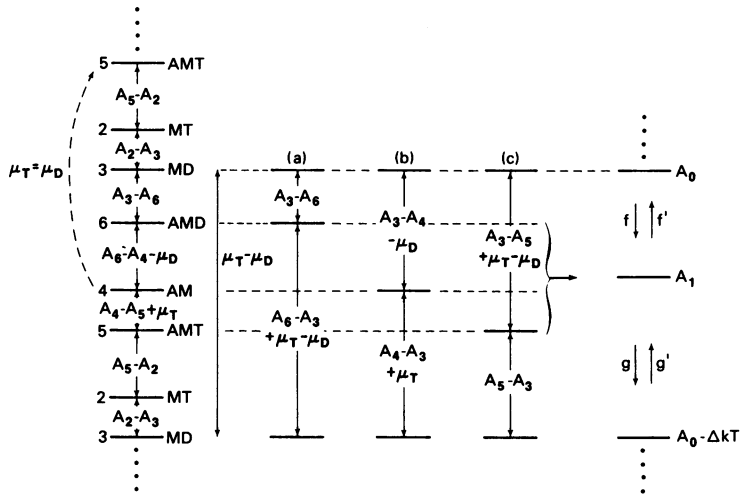

FIGURE 2 Free energy level differences between states in the dominant cycle of Fig. 1 and in the reduced two-state cycle. See text for further details.

nothing to do with the "concentration" of cross-bridges or of actin sites in this structure (if, say, one tries to make an analogy with free *S*1 or *HMM* molecules in solution). The chemical potentials appear in Eqs. 1 and 5, but not in Eqs. 2–4, because state 4 (*AM*) is the only state (in this cycle) in which the cross-bridge does not contain bound nucleotide. The equilibrium constants are for "isomeric" reactions (changes in state of the cross-bridge), and are dimensionless. Note that, if c_T and/or c_D are varied, $\alpha_{45}/\alpha_{54} \sim c_T$, $\alpha_{64}/\alpha_{46} \sim 1/c_D$, but the other rate constant ratios are unaffected.

A schematic but possible set of free energy levels for these five states is shown at the left of Fig. 2. The free energy differences are indicated. In this illustration, there is a drop in free energy for every counterclockwise step in the cycle, but this need not be the case. However, one *complete* cycle (starting at any state) must give a *total* drop of $\mu_T - \mu_D$. The order of magnitude of this quantity, in vivo, is about 10–13 kcal · mol^{-1} (see section 4). When $\mu_T \neq \mu_D$, the free energy levels can be extended indefinitely above and below the levels actually shown in the figure (which refers to the case $\mu_T > \mu_D$), one set 23645 for each cycle. But in the special case of equilibrium, where the (extremely small) ATP concentration c_T^e is chosen to be in equilibrium with c_D (whatever its value, so long as it is finite), we have $\mu_T = \mu_T^e$ and $\mu_T^e - \mu_D = 0$. In this case the free energy "drop" $A_4 - A_5 + \mu_T^e$ will lead back (dashed arrow) to the top level (state 5 = *AMT*) shown in the figure. At equilibrium, then, there is only a single set of five free energy levels instead of the nonequilibrium indefinite set.

The mathematical equivalents of the above comments on the complete cycle are, from Eqs. 1–5,

$$K_{45} \cdot K_{52} \cdots K_{64} = (\alpha_{45}/\alpha_{54}) \cdots (\alpha_{64}/\alpha_{46}) = e^{(\mu_T - \mu_D)/kT} \equiv e^{\Delta} \qquad (7)$$

and

$$K_{45}^e \cdot K_{52} \cdots K_{64} = (\alpha_{45}^e/\alpha_{54}^e) \cdots (\alpha_{64}/\alpha_{46}) = e^{(\mu_T^e - \mu_D)/kT} = 1, \quad (8)$$

where Δ is defined as $(\mu_T - \mu_D)/kT$ and Eq. 8 refers to the equilibrium case mentioned above in which $c_T = c_T^e$. If, for example, $e^\Delta = 10^{10}$ (section 4), the *average* K_{ij} or α_{ij}/α_{ji} in Eq. 7 would be 10^2 (there being five steps in the cycle).

If we wish to consider explicitly variations in both c_T and c_D, we can write, from Eqs. 6,

$$e^\Delta \equiv e^{(\mu_T - \mu_D)/kT} = (c_T/c_T^e)/(c_D/c_D^e) = (c_T/c_D)/(c_T^e/c_D^e), \quad (9)$$

where c_T^e, c_D^e is any equilibrium pair of values. For example, if we take 10^{10} as the in vivo value of e^Δ, the in vivo ratio c_T/c_D is 10^{10} times as large as the equilibrium ratio c_T^e/c_D^e.

Of course the cycle in Fig. 1, or a similar one, may also apply to free *HMM* or *S*1 in solution, in the presence of ATP, products, and *F*-actin. But the definitions of rate constants, equilibrium constants, and free energy changes, as well as their physical interpretations, are different in such a system (Hill, 1975*b*). The interrelationships between the "structural" and "solution" systems is a subject for future investigation (see Hill, 1974, pp. 323–325).

(c) Reduced Two-State Cycle

We now use the cycle in Fig. 1 to illustrate reduction to only two states. We suppose that only one unattached state is important (*MD, MT* or a "fast" equilibrium mixture of *MD* and *MT*), and this state is designated 0. Similarly, there is, we assume, only one significant attached state, designated 1. The single "reduced" attached state might be *AMD, AM, AMT,* or a fast equilibrium mixture of from two to four consecutive states in Fig. 1 that includes at least one attached state and excludes at least one unattached state. The conditions on the rate constants necessary to achieve this kind of reduction to two states are illustrated in Hill (1975*a*, Appendix 2).

A two-state *cycle* remains (Fig. 3): the attachment rate constant in the (dominant) counterclockwise direction is designated f, with inverse f', and the detachment rate constant in the same direction is designated g, with inverse g'. At the detailed molecular level, the respective inverses must of course undo exactly those events (Fig. 1) included in f and g.

The middle of Fig. 2 illustrates some of the specific possibilities for the relative free energy levels of the two states. State 0 is chosen as *MD* here (it could just as well be *MT*), while state 1 is either (*a*) *AMD*, (*b*) *AM*, or (*c*) *AMT*. All three of these cases assume that the eliminated states are transient intermediates (Hill, 1975*a*, Appendix 2). In the event of reduction of a group of states by a fast equilibrium, the single resulting effective state has a lower free energy than any of the individual participants in the equilibrium. For example, for two states $a \rightleftharpoons b$, the free energy A_{ab} for the combined

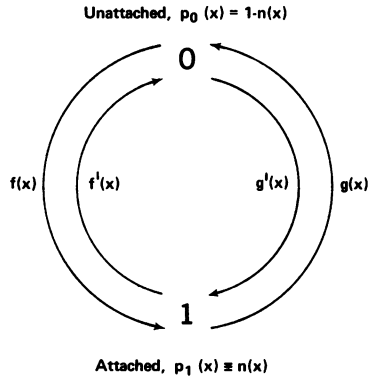

FIGURE 3 Kinetic diagram for two-state models, with first-order rate constants (functions of x). $n(x)$ is the probability of attachment at x.

state ab is given by

$$e^{-A_{ab}/kT} = e^{-A_a/kT} + e^{-A_b/kT}. \tag{10}$$

Cases of this type are not included in Fig. 2 (or Eqs. 14 below).

As indicated on the right of Fig. 2, we designate (whatever the special case) the free energy levels of the two reduced states by $A_0, A_1, A_0 - \Delta kT$, etc., though of course only differences $A_0 - A_1$, etc., have physical significance. Corresponding to Eqs. 1–5, we now have

$$K_{01} = f/f' = e^{-(A_1 - A_0)/kT} \tag{11}$$

$$K_{10} = g/g' = e^{-(A_0 - A_1 - \Delta kT)/kT} \tag{12}$$

Also,

$$K_{01}K_{10} = fg/f'g' = e^{\Delta} = (c_T/c_T^e)/(c_D/c_D^e). \tag{13}$$

Eq. 11 follows directly from detailed balance at "equilibrium," even though $\Delta \neq 0$ (imagine the g, g' transitions to be blocked). That is, $e^{-A_1/kT}$ is proportional to the equilibrium population of state 1, etc. A similar statement applies to Eq. 12. Blockage of either f, f' or g, g' does not change the other two rate constants or the free energies. Hence it is legitimate to use the equilibrium situation as a device to establish the connections in Eqs. 11 and 12.

If c_T and/or c_D are to be varied, the effect of these variables on f/f' and g/g' depends on the special case, as is evident from Fig. 2 (note μ_T and μ_D in the free energy differences). For the different cases in the figure (not the only possibilities):

$$\begin{aligned} &\text{(a)}\quad f/f' \sim \text{const}, \qquad g/g' \sim c_T/c_D \\ &\text{(b)}\quad f/f' \sim 1/c_D, \qquad g/g' \sim c_T \\ &\text{(c)}\quad f/f' \sim c_T/c_D, \qquad g/g' \sim \text{const}. \end{aligned} \tag{14}$$

But in any case, $fg/f'g' \sim c_T/c_D$ (Eq. 13).

The *separate* dependences of f, f', g, and g' on c_T and c_D is a more complicated question that is reserved for the Appendix (see also Hill, 1975*a*, Appendix 2).

3. SUMMARY OF THE FORMALISM FOR TWO-STATE MODELS

With section 2 as background, we turn next to the formalism for two-state models. We give results here, but not derivations. Also, it should be noted, we do not employ the dimensionless notation introduced in the first two papers of this series (Chen and Hill, 1974; Hill and Chen, 1974).

As implied by the term "formalism," we need not make particular commitments as to the molecular origin or biochemical interpretation of the parameters and states which appear in the discussion that follows (see, however, sections 2 and 4).

Each cross-bridge in the ensemble of cross-bridges (section 2) may, we assume here, be in one of two possible biochemical states: state 1 = attached to the (nearest) actin site; state 0 = unattached. The longitudinal location of the nearest attachable actin site relative to a given cross-bridge is specified by a variable x (Fig. 4). In the whole ensemble of cross-bridges, at any instant, as a consequence of the lack of register between the natural spacings on the myosin and actin filaments, there is a *uniform* distribution of x values over an interval of length d, where d is the distance between successive actin sites (on an actin filament) to which a cross-bridge may attach. The obvious value to use for d, incidentally, is the actin filament repeat distance of 360 Å. The considerations of section 2 now apply *at each* x (of course c_T, c_D, and Δ are independent of x). That is, in general, free energies and rate constants are functions of x (details below).

Let $F_1(x)$ be the longitudinal component of the force exerted by the cross-bridge on the actin filament when the cross-bridge is attached (state 1) to the actin site at x (Fig. 4). The origin, $x = 0$, is chosen (by convention) as the point at which $F_1 = 0$. Of course for state 0, $F_0 = 0$ for all x (since the cross-bridge is unattached). The question of force did not arise in section 2 because variations in x were omitted.

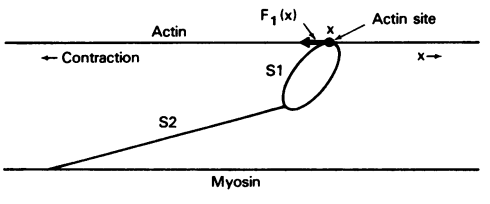

FIGURE 4

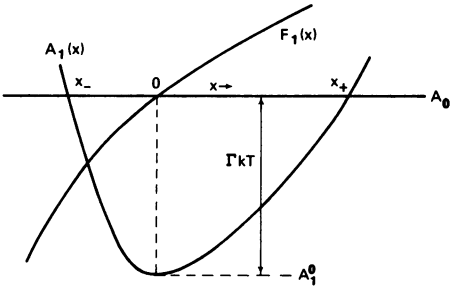

FIGURE 5

FIGURE 4 Schematic myosin cross-bridge attached to actin site at x.
FIGURE 5 Schematic free energy and force functions for a two-state model.

Fig. 3 shows the kinetic diagram for this two-state system. There are four first-order rate "constants," each (in general) a function of x.

In order for this system to work as a free energy transducer (ATP free energy → mechanical work), it is essential to have *two* pairs (f,f' and g,g') of rate constants in the diagram, that is, a *cycle* (reduction of a larger diagram, with one or more cycles, to two states will always produce a two-state cycle). This allows the necessary transient or steady nonequilibrium cyclic flux around the diagram, driven by the high concentration (i.e., far above the equilibrium value) of ATP in solution. Eq. 13 is pertinent in this connection.

The physiological or in vivo value of e^{Δ}, which we denote by e^{Δ_P}, is somewhat uncertain but it is probably between 10^8 and 10^{11} (see section 4). For example, at 3° C, if $e^{\Delta_P} = 10^8$, then $\Delta_p = 18.4$ and $\mu_T - \mu_D = 10.1$ kcal · mol^{-1}. Or, if $e^{\Delta_P} = 10^{10}$, $\Delta_p = 23.0$ and $\mu_T - \mu_D = 12.6$ kcal · mol^{-1}.

(a) Self-consistency

A crucial point, which we now turn to, is that the functions F_1, f, f', g, and g', introduced above, are not independent of each other. Assignment of these functions in the construction of a two-state model without being aware of this fact will in general produce a model that lacks self-consistency.

An unattached cross-bridge (state 0) has a free energy, denoted by A_0, that is independent of x. When attached (state 1), the cross-bridge free energy is a function of x, $A_1(x)$. Since $F_1 = \partial A_1/\partial x$ (Hill, 1974), $A_1(x)$ is determined by $F_1(x)$ (if already specified), except for an integration constant:

$$A_1(x) = A_1^0 + \int F_1(x)\,dx. \tag{15}$$

A_1^0 is the value of A_1 at $x = 0$. As an illustration of Eq. 15, if

$$F_1(x) = Kx + ax^2 + \cdots, \tag{16}$$

then

$$A_1(x) = A_1^0 + \frac{1}{2}Kx^2 + \frac{1}{3}ax^3 + \cdots, \tag{17}$$

where K is the (Hooke's law) force constant. A schematic illustration is shown in Fig. 5. Since $F_1 = 0$ at $x = 0$, A_1 necessarily has a minimum, $A_1 = A_1^0$, at $x = 0$ (this is the position of the actin site that provides the most stable attachment of the cross-bridge). The free energies of the two states are equal at $x = x_-$ and $x = x_+$ (Fig. 5). Between these values of x, $A_1 < A_0$ and the attached state is thermodynamically more stable. But outside of x_- and x_+, the unattached state is more stable.

We define $\Gamma = (A_0 - A_1^0)/kT$. ΓkT is the maximum free energy of detachment (Fig.

5). The magnitude of Γ relative to Δ has an important bearing on the efficiency and other properties, as might be expected (see below).

We see from Eq. 11 that the ratio f/f' at any x is determined by the free energy difference $(A_1 - A_0)/kT$ at that x. Hence only one of the two functions $f(x)$ and $f'(x)$ can be assigned with complete freedom if, for example, $F_1(x)$ is already specified. When $A_1 = A_0$, that is, at $x = x_-$ and x_+, we must have $f = f'$. When $A_0 > A_1$ (attached state more stable), that is, between x_- and x_+, we have $f > f'$ (the rate constant leading toward the more stable state is the larger). Also, when $A_1 > A_0$ (unattached state more stable), that is, outside of x_- and x_+, we have $f' > f$. Some of these points are included in Figs. 6*a*–6*e*, especially Fig. 6*d*.

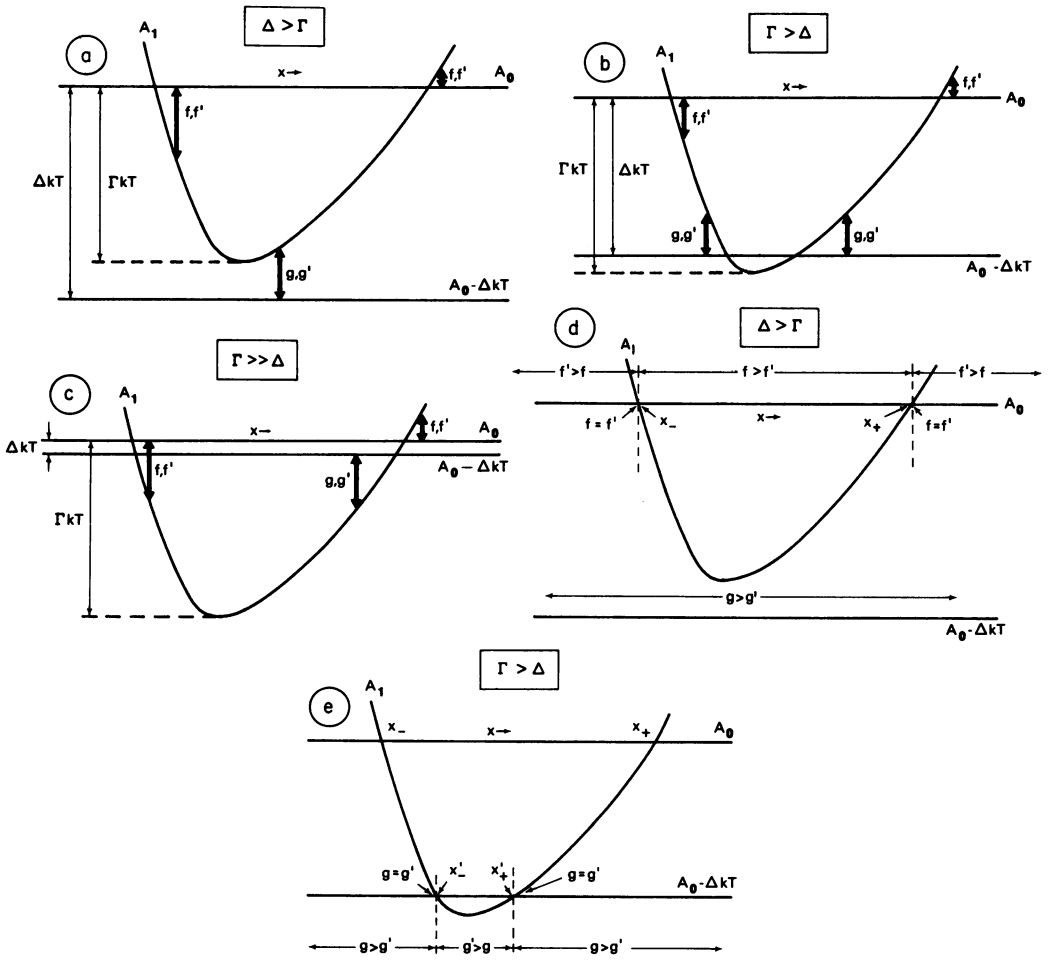

FIGURE 6 (*a*) Schematic free energy levels for a two-state model ($\Delta > \Gamma$) showing relationship of transition pairs to these free energy levels. (*b*) The case $\Gamma > \Delta$. (*c*) The case $\Gamma \gg \Delta$ (near equilibrium). See text. (*d*) Relative magnitude of rate constants as a function of $x(\Delta > \Gamma)$. (*e*) The case $\Gamma > \Delta$.

According to Eq. 12 and Figs. 6*a*–6*e*, the ratio $g'(x)/g(x)$ has the same relation to $A_1(x) - (A_0 - \Delta kT)$ that $f(x)/f'(x)$ has to $A_1(x) - A_0$. For example, only one of g' and g can be independent if $A_1 - (A_0 - \Delta kT)$ is already specified. When $A_1 = A_0 - \Delta kT, g = g'$ (at $x = x'_-$ and x'_+ in Fig. 6*e*); etc. If g' is assumed in a model to be small or negligible compared to g, for all x, it is clearly necessary to use $\Delta > \Gamma$ (compare Figs. 6*d* and 6*e*). Very near to equilibrium ($\Gamma \gg \Delta$), Fig. 6*b* degenerates into Fig. 6*c*. In this example, Fig. 6*b* → 6*c*, we have assumed that only g and g' change as $\Delta \to 0$ (see below).

The concentration dependence of $f(x)/f'(x)$ (as in Eqs. 14) is contained entirely in $e^{-(A_1^\dagger - A_0)/kT} = e^{\Gamma}$ (see Eq. 11) since $\int F_1(x)\,dx$ in Eq. 15 does not involve c_T or c_D. That is, the *shape* of $A_1(x)$ does not depend on these concentrations since this shape has to do solely with the intrinsic macromolecular properties of a cross-bridge attached to an actin site (Hill, 1974, section II). An alternative but equivalent statement is that μ_T and μ_D in Fig. 2 have the same values for all x. Similarly, the concentration dependence of $g(x)/g'(x)$ (as in Eqs. 14) is contained entirely in the factor $e^{-(A_0 - A_1^\dagger - \Delta kT)/kT} = e^{\Delta - \Gamma}$. The variation $e^{\Delta} \sim c_T/c_D$ is general but the possible dependence of e^{Γ} on c_T and/or c_D may be different in different cases.

In summary: specification of the force function $F_1(x)$ determines $A_1(x) - A_0$ to within a constant (ΓkT); this free energy difference, in turn, determines the rate constant ratios $f(x)/f'(x)$ and (with ΔkT) $g'(x)/g(x)$. Thus the parameters of a self-consistent two-state model ($F_1, f, f', g, g', \Gamma, \Delta$) are fairly tightly interconnected.

(b) Steady Isotonic Contractions

Fig. 7*a* (solid arrowed path) illustrates the transition details in one particular hypothetical "pass" of an actin site by a cross-bridge in a steady isotonic contraction. The site approaches the cross-bridge (in state 0) from large positive x (arrows), recedes from the cross-bridge (again in state 0) at large negative x, and at intermediate x interacts with the cross-bridge via f, f', g, g' transitions. In the figure, these transitions are superimposed on the corresponding free energy levels of the two states. The net effect of the six transitions shown in this example (solid arrowed path) is the hydrolysis of one molecule of ATP (counted by the r values) and the performance of a certain amount of work (as measured by the net free energy drop in the segments marked X, Y, and Z). The attachment transition (f) at negative x may be relatively improbable but is included for purposes of illustration. The chemical free energy lost is ΔkT (since $r = 1$ in this example). The dashed path shows a second possible hypothetical sequence with two molecules of ATP hydrolyzed ($r = 2$), that is, with two net cycles completed in Fig. 3.

Fig. 7*a* clearly relates to a stochastic approach to this problem. To compute average measureable quantities such as the mean value of r per pass ($\bar{r}$), the mean work done per pass, etc., one would have to average over thousands of such passes using a Monte Carlo technique. For two-state systems, a much simpler computational approach is to solve the differential equation below.

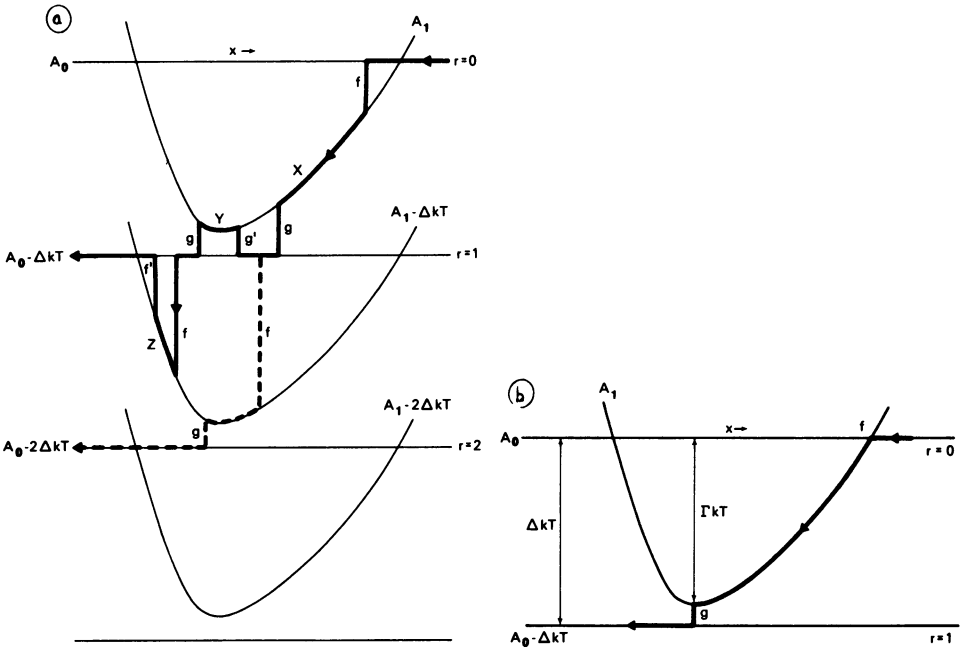

FIGURE 7 (*a*) Schematic set of possible transitions (with one net cycle, $r = 1$) in a single pass of an actin site by a cross-bridge. The dashed path shows a second possible example (with two net cycles, $r = 2$). (*b*) Transitions giving optimal efficiency of Γ/Δ.

The thermodynamic efficiency η is the stochastically averaged work performed per pass (see X, Y, Z, for example, in Fig. 7 *a*) divided by $\bar{r}\Delta kT$. When $\Delta > \Gamma$, it is clear from Fig. 7 *b* that there is no way (i.e. for any choice of the other parameters) that the efficiency could be greater than Γ/Δ.

The probability that a cross-bridge, with nearest actin site at x, is in state 1 (attached) is $p_1(t,x) \equiv n(t,x)$ and in state 0, $p_0(t,x) = 1 - n(t,x)$. In steady motion, n is a function of x only. The differential equation that determines $n(x)$ in steady motion is (Fig. 3)

$$\mathrm{d}n/\mathrm{d}t = (\partial n/\partial t)_x + (\partial n/\partial x)_t(\mathrm{d}x/\mathrm{d}t) = -v(\mathrm{d}n/\mathrm{d}x)$$
$$= [f(x) + g'(x)][1 - n(x)] - [f'(x) + g(x)]n(x), \qquad (18)$$

where $v = -\mathrm{d}x/\mathrm{d}t$ is the velocity of contraction and $(\partial n/\partial t)_x = 0$ (steady motion).

Having found $n(x)$ by solving Eq. 18 for a given v, the mean force exerted on the actin filament at this v, per cross-bridge in the overlap zone, is then

$$\bar{F} = \frac{1}{d}\int_{-\infty}^{+\infty} F_1(x)n(x)\mathrm{d}x. \qquad (19)$$

Here we use the fact, mentioned earlier, that there is a uniform distribution in x values

within the ensemble of cross-bridges. The limits $\pm\infty$ can be introduced instead of $\pm d/2$ (Hill, 1974, p. 285) since necessarily $n(x) = 0$ at $x = \pm d/2$ (to be consistent with the single actin site assumption made at the outset). The appropriateness of averaging over an interval d can be seen most easily by considering an indefinite array of actin sites at intervals d, with one arbitarily chosen site assigned the location x (Hill, 1975*a*, section IVC). Then $n(x)$, the probability of attachment to *any* site, is periodic in x with period d.

The mean rate of hydrolyzing ATP molecules, per cross-bridge, is

$$\bar{J} = \frac{\bar{r}v}{d} = \frac{1}{d}\int_{-\infty}^{+\infty} \{g(x)n(x) - g'(x)[1 - n(x)]\}\,dx. \tag{20}$$

Alternatively, $f(1-n) - f'n$ can be used as the integrand. The efficiency is

$$\eta = \frac{\text{mean rate of doing work}}{\text{mean rate of use of ATP free energy}} = \bar{F}v/\bar{J}\Delta kT \tag{21}$$

$$= \frac{\text{mean work per pass}}{\text{mean ATP free energy use per pass}} = \bar{F}d/\bar{r}\Delta kT. \tag{22}$$

(c) Very Near Equilibrium

In the domain of irreversible thermodynamics (which is of considerable theoretical but no physiological interest), $\bar{F}$ and $\bar{J}$ in Eqs. 19 and 20 are both linear functions of ΔkT and v:

$$\begin{aligned} \bar{F} &= A(\Delta kT) - Bv + \cdots \\ \bar{J} &= C(\Delta kT) + Dv + \cdots \end{aligned} \tag{23}$$

where the coefficients A, B, C, and D are positive constants that are properties of the system *at equilibrium.* At equilibrium, Δ, v, $\bar{F}$, and $\bar{J}$ are all zero.

We can obtain explicit expressions for A, B, C, and D following the method of Hill (1974, pp. 332–335). But, for consistency with the above discussion of concentration dependence, it is desirable to use here the most general possible variations in the four rate constants near equilibrium:

$$\begin{aligned} f(x) &= f^e(x)(1 + a_1\Delta + \cdots) \\ f'(x) &= f'^e(x)(1 + a_2\Delta + \cdots) \\ g(x) &= g^e(x)(1 + a_3\Delta + \cdots) \\ g'(x) &= g'^e(x)(1 + a_4\Delta + \cdots), \end{aligned} \tag{24}$$

where the a_i are in general functions of x but are subject to certain restraints. First, in view of Eq. 13, we must have $(a_1 - a_2) + (a_3 - a_4) = 1$. Second, since

$$f(x)/f'(x) = [f^e(x)/f'^e(x)]e^{\Gamma - \Gamma^e}, \tag{25}$$

where Γ and Γ^e are independent of x, we have, on comparing Eqs. 24,

$$\Gamma - \Gamma^e = (a_1 - a_2)\Delta \qquad (\Delta \to 0). \tag{26}$$

Therefore the difference $a_1 - a_2$ must be independent of x (likewise $a_3 - a_4$). Using these restraints, one can then show that

$$A = -\frac{1}{dkT}\int_{-\infty}^{+\infty}\frac{n^e F_1 g^e}{\Sigma^e}\,dx \tag{27}$$

$$B = \frac{1}{dkT}\int_{-\infty}^{+\infty}\frac{n^e(1 - n^e)F_1^2}{\Sigma^e}\,dx \tag{28}$$

$$C = \frac{1}{dkT}\int_{-\infty}^{+\infty}\frac{f^e g^e}{\Sigma^e}\,dx \tag{29}$$

$$D = \frac{1}{dkT}\int_{-\infty}^{+\infty}\frac{n^e F_1 f'^e}{\Sigma^e}\,dx, \tag{30}$$

where $\Sigma^e = f^e + f'^e + g^e + g'^e$ and $n^e = (f^e + g'^e)/\Sigma^e$. Note that only equilibrium properties appear in these equations (not the a_i). The Onsager reciprocal relation is $A = D$, and this equality is not difficult to verify from Eqs. 27 and 30. It is useful as a computational check on any model (see section 4).

In previous work we have generally used the special case $g = g^e e^{\Delta}$ (i.e., $a_1 = a_2 = a_4 = 0$, $a_3 = 1$). Eqs. 297 *a, b* of Hill (1975 *a*), with $g = \alpha_T^*$ and $g' = \beta_T^*$, provide a different example: $a_1 = a_2 = 0, a_3 = 1/(1 + a), a_4 = -a/(1 + a)$, where a is a function of x. See also the Appendix.

For a given Δ, the efficiency η is a function of v: $\eta = 0$ at $v = 0$ (section 5 is an exception) and at $v = v_{max}$ (where $\bar{F} = 0$); and η has a maximum value, η^*, at some intermediate $v = v^*$. At equilibrium (i.e. in the limit $\Delta \to 0$), one finds (Hill, 1974)

$$\eta_{eq}^* = 1 - \frac{2BC}{A^2}\left[\left(1 + \frac{A^2}{BC}\right)^{1/2} - 1\right]. \tag{31}$$

For a given model, if A, B, and C are computed from Eqs. 27–29, η_{eq}^* may be compared with η^* calculated under physiological conditions (see sections 4 and 5, and Hill and Chen, 1974).

4. MODIFICATION OF PODOLSKY-NOLAN MODELS

Podolsky and Nolan investigated a large number of two-state models in a search for special cases that would produce isotonic transients (length *vs.* time) similar to those found experimentally (Civan and Podolsky, 1966). Most of these results have not been published. However, from the point of view of section 3, these models (along with most others in the literature) are somewhat suspect: they may be incomplete and lack self-consistency in varying degrees.

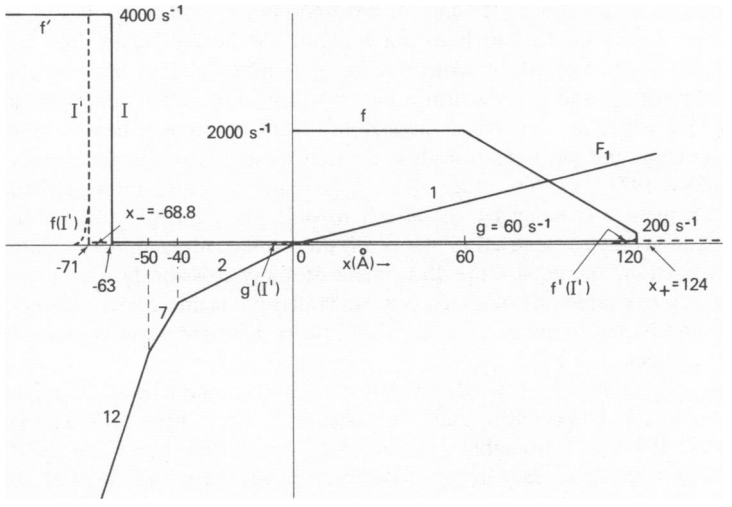

FIGURE 8 Model I of Podolsky and Nolan (solid lines). The dashed curves show the changes needed for model I'. The numbers on F_1 are relative slopes.

We employ three of these Podolsky-Nolan models here (which we denote by I, II, and III) as starting points in the construction of illustrative two-state muscle models that are both complete and self-consistent. In each case (I, II, III) we shall consider the modifications needed in order to establish a "legal" model, according to the prescription in section 3. This procedure will lead to ("legalized") models denoted I', II', and III', respectively. However, model III' is not treated in any detail.

We emphasize that these are examples only. Our primary though not our only objective in this paper is to illustrate the proper application of the formalism. Therefore we have made no attempt in the present work to search systematically for a more or less optimal, self-consistent, two-state model of the Podolsky-Nolan type. It is our impression, however, that such a search would very likely produce a model (probably rather closely related to III) with generally satisfactory properties.

Model I is the model that has been used most extensively by Podolsky and Nolan (1971, 1973). The rate constant f (Fig. 8) is finite between $x = 0$ and $x = 120$ Å. The rate constant f' (Fig. 8) corresponds to the non-ATP-splitting branch of "g" used by Podolsky and Nolan (1973). The properties of models II and III have not been published before (the computations were made in the same way as for model I, as described by Podolsky and Nolan). These latter two models have a finite f between $x = 0$ and $x = 60$ Å. To anticipate the main result below: model I requires significant alteration ($I \rightarrow I'$), but models *II* and *III*, with "narrow f, are practically "legal" as they stand (though not complete).

(a) Background Comments on Podolsky-Nolan Models

Podolsky-Nolan models are a modification of the original cross-bridge model of muscle contraction, first presented by A. F. Huxley (1957). Podolsky and Nolan modified the Huxley

model in order to explain the contraction transients that were observed (Civan and Podolsky, 1966) after the Huxley model had been put forward. Podolsky-Nolan models are two-state models in which the rate of attachment to actin, f, is postulated to be much faster than the rate of detachment, g, and a cross-bridge can reattach immediately after detachment if it is still in a position where an actin site is accessible. That is, no step occurs following detachment that is rate limiting, such as a transition from a refractory to a nonrefractory state (Eisenberg and Kielley, 1973). On the other hand, these models have a rather stringent geometric requirement, namely, a cross-bridge can attach to only one actin per turn of the actin helix. Because of this geometric restriction many of the cross-bridges remain unattached during isometric contraction. In fact, it is the detachment of many cross-bridges for geometric reasons combined with a very rapid rate of attachment when they come into correct position that is used by Podolsky and Nolan to account for the early phase of rapid velocity development during the isotonic transient.

In Podolsky-Nolan models, as in all two-state models, the unattached state might be expected to correspond to the biochemical state that occurs in vitro after ATP binding to myosin (Bagshaw et al., 1974) or presumably to actomyosin as well, that is, MT or MD^* or an equilibrium mixture of the two. MD in Fig. 1 differs from MD^* by some kind of conformational change (Bagshaw et al., 1974). In two-state models, such as those of Podolsky and Nolan, in which g, the rate of detachment, is relatively small, it is unlikely that g corresponds either to $AM + T \rightarrow AMT$ (Fig. 1) or to $AMT \rightarrow A + MT$, both of which have been reported to be very fast (Lymn and Taylor, 1971). Rather it is more likely that g corresponds to $AMD \rightarrow AM + D$, which of course must occur before ATP can rebind to AM. In this case the attached state will be AMD.

The above implies that, in Podolsky-Nolan models, essentially simultaneously with attachment of the cross-bridge to actin, MT or MD^* converts to AMD. This conversion is observed to occur much more slowly with myosin alone than with actomyosin so presumably it is enzymatic in nature. Since, in Podolsky-Nolan models, attachment can occur over a fairly wide range of x (Fig. 8), this enzymatic transition must also be possible over a wide range of x. Also, release of products from AMD (the g process) occurs over a considerable range in x. But in most enzymes, a change in conformation of a few angstroms greatly alters or even abolishes enzymatic properties. Thus, in Podolsky-Nolan models, either in some way x is unrelated to the configuration of the actin-myosin attachment (for example, $S2$ is a spring the length of which adjusts to suit the value of x), or large changes in the attachment configuration do not lead to major changes in enzymatic activity. This is in contrast to many biochemical models in which the biochemical state of the actomyosin is directly related to the actin-myosin attachment configuration, for example to the angle between actin and the cross-bridge.

What does depend strongly on x in Podolsky-Nolan models is the force exerted by the cross-bridge (Fig. 8). As discussed in section 3, this force is related to the change in free energy of the attached state with x, which in turn is related to the change in the f/f' ratio with x. If the rate of attachment, f, changes relatively little as x approaches zero from the positive side, f' must be decreasing by many orders of magnitude (see below). In this case the decrease in free energy of the attached state with x, which is associated with force development in this model, will be tied to a dramatic decrease in f' the rate of detachment of the cross-bridge, rather than to a large increase in the rate of attachment.

One other critical feature of Podolsky-Nolan models is that, in regions of high negative force, the rate of detachment of the cross-bridge from actin increases sharply, but the detachment in this case occurs without the hydrolysis of ATP (the f' process, Fig. 8). As pointed out by Podolsky and Nolan, this feature is necessary both to account for the duration of the slow phase of the isotonic transient and to satisfy the Fenn effect. If the model is correct in regions of high negative force, AMD will have an altered conformation that somehow favors the f' pro-

cess (inverse of f) over the g process ($AMD \rightarrow AM \rightarrow AMT \rightarrow MT$ or MD^*). Although in both the original Huxley (1957) and Podolsky-Nolan models negative force occurs, only in the latter case in this negative force associated with an altered conformation in AMD that leads to detachment without ATP hydrolysis occurring.

As we shall see below, because of this assumption of a large f' at negative x, particular restrictions are placed on f and f' by the force function used. It is this feature that makes model I (below) "illegal" as it was originally presented.

(b) Models I and I'

Fig. 8 shows model I (solid lines): $f' = 4{,}000\ s^{-1}$ for $x \leq -63$ Å; $g = 60\ s^{-1}$ for -63 Å $\leq x \leq 120$ Å; f is finite in the interval $0 \leq x \leq 120$ Å as shown; $g' = 0$ everywhere; and the force function $F_1(x)$ for the attached state is

$$\begin{aligned} F_1(x) &= Kx && (x \geq 0) \\ &= 2Kx && (-40 \leq x \leq 0) \\ &= K(7x + 200) && (-50 \leq x \leq -40) \\ &= K(12x + 450) && (-\infty \leq x \leq -50). \end{aligned} \tag{32}$$

Units of angstroms for x are omitted but understood from this point on. The numbers on F_1 in Fig. 8 are the relative slopes of the different segments. The isotonic transients obtained from this model (Podolsky and Nolan, 1971, 1973) are close to those seen experimentally. The steady force-velocity curve, which we have recalculated from Eqs. 18 and 19, also compares favorably with experiment (circles in Fig. 9), except at small values of $\bar{F}/\bar{F}_0$ (where $\bar{F}_0$ = isometric force).

We now examine model I for self-consistency. As will be explained below, there is a conflict between the selected f and f' on the one hand and F_1 and Eq. 11 on the other.

Free Energy Function. The first step is to obtain the free energy function from Eqs. 15 and 32. At positive x, we have

$$A_1/kT = (A_1^0/kT) + (x^2/2\sigma^2) \qquad (x \geq 0) \tag{33}$$

where we have replaced K by kT/σ^2. These parameters are interchangeable. The function $e^{-A_1/kT}$, which occurs, for example, in Eqs. 11 and 12, is Gaussian at positive x, with standard deviation σ (in Å).

In the next interval (Eq. 32), integration gives

$$A_1/kT = (A_1^0/kT) + (x^2/\sigma^2) \qquad (-40 \leq x \leq 0). \tag{34}$$

This choice of integration constant makes A_1/kT continuous at $x = 0$. In the third interval (Eq. 32), the integration constant is evaluated by requiring continuity of A_1/kT at $x = -40$. The same requirement is imposed at $x = -50$ for the fourth in-

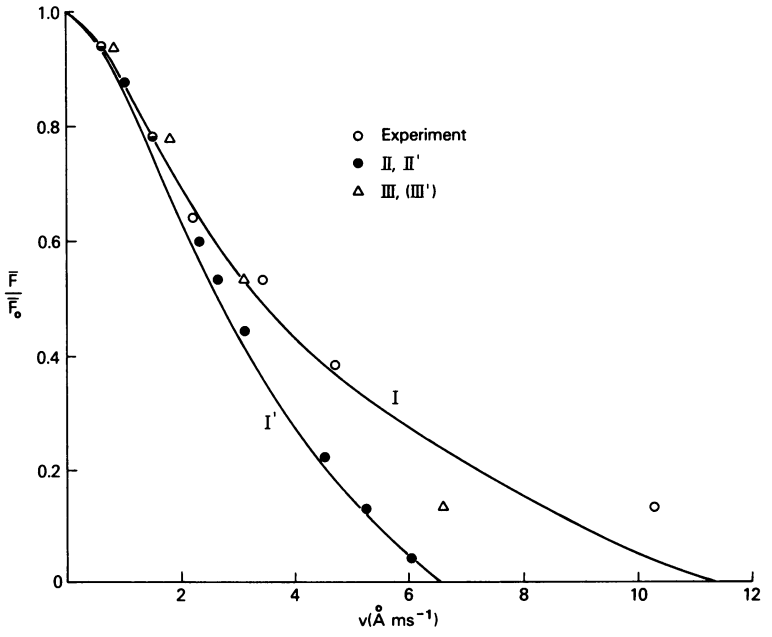

FIGURE 9 Relative force vs. velocity in steady isotonic contractions. The solid curves have been computed from models I and I'. Included are experimental points (○) (Civan and Podolsky, 1966), points calculated from models II and II' (●) (identical on this scale), and points from model III (△) (model III' is presumed to give essentially the same results as model III).

terval. Thus we find

$$A_1/kT = (A_1^0/kT) + (1/\sigma^2)\left(\frac{7}{2}x^2 + 200x + 4000\right) \quad (-50 \leq x \leq -40)$$
$$= (A_1^0/kT) + (1/\sigma^2)(6x^2 + 450x + 10250) \quad (-\infty \leq x \leq -50). \tag{35}$$

Values of x_+ and x_-. Since $A_0 = A_1$ at x_+ and x_-, we have from Eq. 33

$$(A_0 - A_1^0)/kT = \Gamma = x_+^2/2\sigma^2 = \phi(x_-)/\sigma^2, \tag{36}$$

where $\phi(x)$ is the polynomial in the particular branch of A_1/kT at negative x (Eqs. 34 and 35) that includes x_-. We note that the relation between x_+ and x_- is $x_+^2/2 = \phi(x_-)$ irrespective of the choices of Γ and σ, and that if, say, x_+ and Γ are assigned values, then σ (or K) is automatically fixed.

It is easy to show that, for any two-state model (see Eq. 16), the relation between x_+ and x_- is completely determined by the force function $F_1(x)/K$.

In model I, f' is assumed to be zero at positive x. This requires that $x_+ > 120$. For, if $x_+ < 120$, we would have $f' > f$ in the interval $x_+ \leq x \leq 120$, according to Eq. 11 and Fig. 6*d*. There is no problem in the region $x > 120$, by the way, since we imagine *both* f and f' to be negligibly small there, whatever their ratio as determined

by Eq. 11. This is done largely for convenience, for it would also be possible for f' to be quite large in this region, with $f' \gg f$ (see, for example, Fig. 13, below).

Consider the value $x_+ = 124$, as an example. From $x_+^2/2 = \phi(x_-)$, we find $x_- = -68.8$. But this contradicts the requirement $x_- > -63$ (if $x_- < -63$, we would have $f > f'$ in the interval $x_- \leq x \leq -63$, whereas we have assumed $f = 0$ at negative x). Incidentally, if we should take $x_+ = 120$ (which is itself unsatisfactory since it makes $f' = f = 200\ s^{-1}$ at $x = 120$), we would have $x_- = -67.5$, which still violates $x_- > -63$.

Clearly, the origin of this problem with model I is that the pair of critical values $x = -63$ and $+120$ (Fig. 8) in the f' and f functions, respectively, are not consistent with the chosen force function F_1/K (Eq. 32). We need both x_+ to the right of the f function (Fig. 8) and x_- to the right of the f' function, and F_1/K does not allow this. Note that this problem would not arise in any model that has $f' = 0$ at negative x (there are two examples in section 5).

Model I'. We now alter model I not only to make it self-consistent but also complete (e.g., the efficiency cannot be calculated for model I as it stands). The modification we use alleviates but does not entirely eliminate the above difficulty with f and f'. At the same time, the function g' (which is relatively unimportant—except possibly at or near equilibrium) is introduced. The change adopted for f, f' is to take $x_+ = 124$ and move the position of the step in f' from $x = -63$ to $x = -71$ (that is, to the left of $x_- = -68.8$), as shown by the dashed vertical line in Fig. 8. Alternatively, the cut-off in f at $x = 120$ could have been moved in to about $x = 97$, or the slope of F_1 for $x < -50$ could have been increased by a factor of about five, or a compromise between these three changes could have been employed. In any case (see below for model I'), fairly severe effects on model properties can be anticipated.

With the choice $x_+ = 124$, and retention of f as in model I, Eq. 11 still requires a nonnegligible f' function near $x = 120$. This is the dashed curve labeled $f'(I')$ in Fig. 8 (details below). Similarly, the step in f' at $x = -71$ together with $x_+ = 124$ and Eq. 11 leads to the nonnegligible, dashed $f(I')$ curve near $x = -71$. To eliminate $f'(I')$ would require $x_+ > 124$, but this in turn would necessitate $x_- < -68.8$ and corresponding relocation of the f' step at $x < -71$. The $f(I')$ function in Fig. 8 could be avoided simply by shifting the f' step to the left of the $f(I')$ curve (leaving $x_- = -68.8$). But increasing the f, f' "gap" from 63 Å to 71 Å is already too drastic for satisfactory mechanical properties (see below). Therefore further increase in the gap, to eliminate $f'(I')$ and/or $f(I')$, would not be helpful.

In the gap ($-71 \leq x \leq 0$), as in the region $x > 120$, we consider *both* f and f' to be negligibly small, and so we can ignore the requirements of Eq. 11.

To proceed further, we must now consider Δ_p (the only value of Δ used below, except $\Delta \rightarrow 0$) and Γ. As in our previous papers (Hill, 1974; Hill and Chen, 1974), we have adopted for our calculations $e^{\Delta_p} = 10^8$, though recent work suggests that, say, 10^{10} might be a better choice (see below). At $x = 0$, Eq. 12 becomes

$$e^{\Gamma}/e^{\Delta_p} = g'(0)/g(0). \tag{37}$$

Since g' is omitted entirely from model I, to avoid unnecessary alteration of this model we want $g' \ll g$ in model I'. We see from Eq. 37 and Figs. 6*d* and 6*e* that we need $\Delta_p > \Gamma$ for this purpose. However, as pointed out in connection with Fig. 7*b*, if Γ is too small relative to Δ, the efficiency will be adversely affected. Since $g = 60\ s^{-1}$ is already a relatively small rate constant, we adopt as a compromise $e^{\Gamma} = 10^7$, so that $g'(0) = g(0)/10 = 6\ s^{-1}$ (Fig. 8). On either side of $x = 0, g'(x) \rightarrow 0$ in accordance with Eqs. 12 and 33–35. The maximum conceivable efficiency (Fig. 7*b*), Γ/Δ, is then 0.875.

Incidentally, in model I' (Fig. 8), we extend $g = 60\ s^{-1}$ to $x = -71$ and also to $x > 120$ (this latter is needed only if calculations are made at or near equilibrium).

Having selected $x_+ = 124$ and $e^{\Gamma} = 10^7$, Eq. 36 gives $\sigma = 21.84$ Å. This same order of magnitude for σ was used on pp. 275 and 310 of Hill (1974). The value of $K = kT/\sigma^2$ at 3°C is then 0.80 erg · cm^{-2}. This result is discussed under (*f*) below.

To complete the specification of model I', we give the explicit dashed functions shown in Fig. 8. These follow from Eqs. 11, 12, and 33–35:

$$\begin{aligned} f'(I') &= \frac{(-30x + 3800)s^{-1}}{10^7\, e^{-x^2/2\sigma^2}} && (60 \le x \le 120) \\ &\cong 0 && (0 \le x \le 60) \end{aligned} \tag{38}$$

$$\begin{aligned} g'(I') &= 6e^{-x^2/2\sigma^2}\, s^{-1} && (x \ge 0) \\ &= 6e^{-x^2/\sigma^2}\, s^{-1} && (-40 \le x \le 0) \\ &\cong 0 && (x < -40) \end{aligned} \tag{39}$$

$$f(I') = 4000 \exp[\Gamma - (1/\sigma^2)(6x^2 + 450x + 10250)]s^{-1} \qquad (x \le -71) \tag{40}$$

Incidentally, the value of $f'(I')$ at $x = 120$ is $72\ s^{-1}$ (compared with $f = 200\ s^{-1}$), and the value of $f(I')$ at $x = -71$ is $662\ s^{-1}$ (compared with $f' = 4000\ s^{-1}$).

Effect of Δ_p Value. As mentioned in section 3, $e^{\Delta_p} = 10^8$ at 3°C corresponds to $\mu_T - \mu_D = 10.1$ kcal · mol^{-1}. Higher values for this latter quantity are suggested by Kushmerick and Davies (1969) and by Curtin et al. (1974). A compromise between these two papers would be $e^{\Delta_p} = 10^{10}$ and $\mu_T - \mu_D = 12.6$ kcal · mol^{-1}. If we had used $e^{\Delta_p} = 10^{10}$ and $e^{\Gamma} = 10^9$ [rather arbitrarily, to retain $g'(0) = g(0)/10$] in our calculations, the effect would be quite small except for a uniform change in magnitude of the force, since $\sigma^{-2} \sim K \sim \Gamma$ (see Eqs. 36 and 47). The main modification contained in model I', the shifting of the f' step from $x = -63$ to $x = -71$, would be unaffected (since the x_-, x_+ relationship depends only on F_1/K). But the $f'(I')$ and $f(I')$ functions would be diminished some in magnitude. Thus, at $x = 120$, $f'(I')$ would become $54\ s^{-1}$ instead of $72\ s^{-1}$ (above) and at $x = -71$, $f(I')$ would become $396\ s^{-1}$ instead of $662\ s^{-1}$.

Computed Results. We turn now to the calculated properties of models *I* and *I'*, ob-

tained by computer from Eqs. 18–21. The force-velocity curves, $\bar{F}/\bar{F}_0$ vs. $v(\text{Å} \cdot \text{ms}^{-1})$, are the two solid curves in Fig. 9. These should be compared with the experimental points (circles). It is apparent that the change in models $I \rightarrow I'$, required to achieve self-consistency, has produced a force-velocity curve (I') that is no longer in reasonable agreement with experiment. The lowering of the I' curve (at higher velocities) can be attributed primarily to the increase in the gap from 63 Å to 71 Å. Because of this discrepancy between model I′ and experiment, we have not thought it worthwhile to compute isotonic transients for this model.

In contrast to the force, the ATP flux vs. velocity curve is practically the same for models I and I′. The force, flux, cycles per pass, and efficiency for model I′ are shown as the solid curves in Fig. 10. The maximum efficiency, η^*, at $v^* \cong 2.5$ Å ms^{-1}, is just under 12%. The value of v_{max} ($\bar{F} = 0$) is 6.4 Å ms^{-1}. The mean number of cycles per pass at v^* is $\bar{r} \cong 3.4$ (compare Figs. 7 *a* and 7 *b* where $r = 1$ or $r = 2$).

The early "hump" in the force-velocity curves (Fig. 9), which is also exhibited by the experimental points (also, see Mulieri, et al. [1974]), is presumably due in the models to the changes in slope of F_1 at $x = -40$ and $x = -50$.

The magnitude of the isometric force for all models is discussed under (*f*) at the end of this section.

The fraction of attached cross-bridges for model I′, under isometric conditions, is found to be $\bar{n}_0 = (1/d)\int n_0 dx = 0.32$, if we take $d = 360$ Å. This result is about as ex-

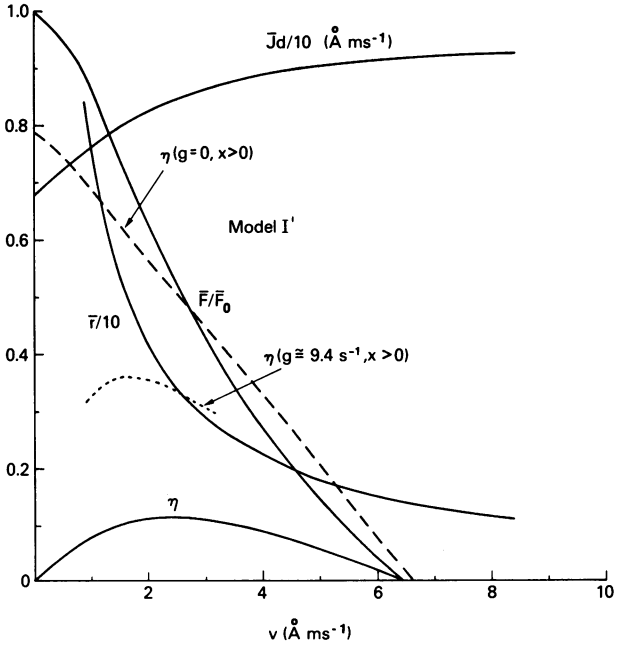

FIGURE 10 Solid curves: computed steady properties of model I′ ($g = 60\ \text{s}^{-1}$). The dashed and dotted curves show the effect on the efficiency of lowering g at $x > 0$.

pected since the f function is 120 Å wide, and $n_0(x) \cong 1$ in that region and is unimportant elsewhere.

Summary on Parameters of the Model. In the original Podolsky-Nolan model (I), rate functions f, g, and f' are given, together with the force function F_1/K. Without regard to self-consistency, the steady properties that may be calculated from these parameters alone are $\bar{F}(v)d/K$ and $\bar{J}(v)d$, as can be seen from Eqs. 15, 19, and 20. By combining these, one can also find $\bar{F}(v)/\bar{F}_0$, $\bar{r}(v) = \bar{J}(v)d/v$, and $\bar{F}(v)v/K\bar{J}(v)$ [the latter quantity, if multiplied by the unspecified constant $K/(\mu_T - \mu_D)$, would give the efficiency]. Absolute values of $\bar{F}(v)$ and $\bar{J}(v)$ are not available.

Starting with the above Podolsky-Nolan ingredients, we have seen that the *additional* parameters needed to make a complete and self-consistent model (I') are the ATP hydrolysis free energy $\Delta_p kT$, the maximum free energy of detachment ΓkT, the distance between effective actin sites d, and the force constant K (or σ, or x_+). We have actually used x_+ rather than K and an experimental value of $\bar{F}_0$ rather than d [see (f), below].

Change of g Value in Model I'. The particular value $g = 60\ s^{-1}$ introduced by Podolsky and Nolan is significant at negative x (in fitting experimental isotonic transients) but is quite arbitrary at positive x. Also, so long as $f \gg g$, the actual value of f in the interval $0 < x < 30$ is arbitrary, since $n \cong 1$ in any case. The choice f = constant in this interval for model I (Fig. 8) was made for convenience.

Since the g value at positive x *does* influence the flux $\bar{J}$ considerably, we examined this effect briefly. To see the maximum effect of reducing g, we repeated our calculations using $g = 0$ at $x > 0$, with no other change except necessarily $g' = 0$ at $x > 0$. With this modification, this model becomes rather similar to the one discussed in section 5.

The computed effect on the force-velocity curve (Fig. 10) is found to be rather small. The effect on the *shape* of the flux curve is also small, but this curve is displaced downward sufficiently to give $\bar{J}_0 = 0$. Zero isometric flux is to be expected here since, at any v, $\bar{J}d = v[n(0) - n(-a)]$, where a is the width of the gap ($a = 71$ Å). This expression is derived in section 5 (Eq. 76). Incidentally, $\bar{r} = n(0) - n(-a) \leq 1$. The dashed curve in Fig. 10 shows the efficiency η as a function of v. The maximum in η is at $v = 0$, as in section 5. The efficiency is seen to have been increased considerably by abolishing g at $x > 0$.

But use of $g = 0$, leading to $\bar{J}_0 = 0$, is certainly unrealistic. Curtin et al. (1974) deduce an experimental value of $\bar{J}_0^{-1} = 0.33_7$ s. Our computed value for model I' ($g = 60\ s^{-1}$) is $\bar{J}_0 d = 6.790$ Å · ms^{-1}. If we use the actin site repeat distance for d, that is, $d = 360$ Å, the experimental value becomes $\bar{J}_0 d = 1.06_8$ Å · ms^{-1}. By interpolation, then, we estimate that $g \cong 9.4\ s^{-1}$ ($x > 0$) for model I' will produce the experimental isometric flux.

Because, as already indicated, the abolishment of g has a rather small effect on both the force and the vertically adjusted flux, we also interpolated "experimental" (i.e., $g \cong 9.4\ s^{-1}$) values of force and flux at several intermediate values of v. The (approximate) efficiency was then calculated and is shown as the dotted curve in Fig. 10.

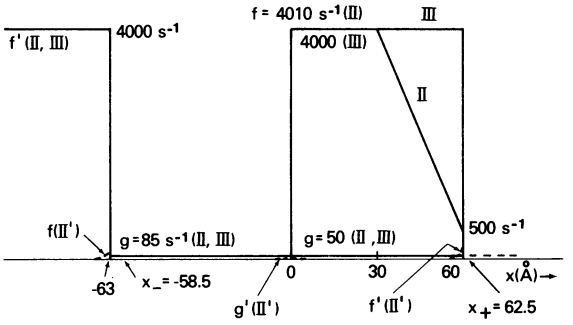

FIGURE 11 Models II and III of Podolsky and Nolan (solid lines). The (barely visible) dashed curves show the changes needed for model II'. The relative slopes 1, 2, 7, 12 in F_1 in Fig. 8 become 1, 1, 2, 4 here, respectively.

We find $\eta^* \cong 0.37$, $v^* \cong 1.7$ Å $\cdot$ ms^{-1}, and $\bar{r} \cong 1.6$ at v^*. This efficiency is of the same order of magnitude as the approximate experimental efficiency of 40–50% (Curtin et al., 1974).

(c) Models II and II'

Model II provides a different kind of example than model I. That is, it does not have significant self-consistency problems. But it does need to be made complete.

Model II (Fig. 11) is of the same type as model I (Fig. 8), but the f function is narrower and larger in magnitude (also, g is altered slightly). The slopes of F_1 shown in Fig. 8 (1, 2, 7, 12) are changed in model II to 1, 1, 2, 4 for the same intervals. Unchanged are the gap of 63 Å and $f' = 4000\ \text{s}^{-1}$ for $x < -63$.

From F_1, we obtain Eq. 33 for the free energy in the region $x \geq -40$. But instead of Eq. 35, we find

$$\begin{aligned} A_1/kT &= (A_1^0/kT) + [(1/\sigma^2)(x^2 + 40x + 800)] \qquad (-50 \leq x \leq -40) \\ &= (A_1^0/kT) + [(1/\sigma^2)(2x^2 + 140x + 3300)] \qquad (-\infty \leq x \leq -50). \end{aligned} \tag{41}$$

The polynomials here give $\phi(x_-)$ in Eq. 36. We then find from $x_+^2/2 = \phi(x_-)$ that if we take, say, $x_- = -58.5$, then $x_+ = 62.52$. That is, unlike model I, we can satisfy both $x_- > -63$ and $x_+ > 60$. Thus, in this case with a narrow f function, the 63 Å gap is already consistent with the chosen F_1/K. Minor additions of $f(II')$, $f'(II')$, and $g'(II')$ (Fig. 11) must still be made to obtain the self-consistent model II', but these have very small effects on computed properties. In other words, model II itself is essentially "legal."

To complete model II', we use the above values of x_+ and x_- together with $e^{\Delta p} = 10^8$ and $e^{\Gamma} = 10^7$ (as for model I'). Eq. 36 then gives $\sigma = 11.01$ Å and $K = kT/\sigma^2 = 3.14$ erg $\cdot$ cm^{-2}. This is about half the value of σ in model I', and four times the value of K (because the width of the f function differs by a factor of two). See (f), below, for further discussion of K.

The new dashed functions in Fig. 11 are

$$f'(II') = \frac{(-117x + 7520)\ \mathrm{s}^{-1}}{10^7\, e^{-x^2/2\sigma^2}} \qquad (30 \le x \le 60)$$

$$\cong 0 \qquad (0 \le x \le 30) \qquad (42)$$

$$g'(II') = 5e^{-x^2/2\sigma^2}\ \mathrm{s}^{-1} \qquad (x \ge 0)$$

$$= 8.5e^{-x^2/2\sigma^2}\ \mathrm{s}^{-1} \qquad (-40 \le x \le 0) \qquad (43)$$

$$\cong 0 \qquad (x < -40)$$

$$f(II') = 4000 \exp[\Gamma - (1/\sigma^2)(2x^2 + 140x + 3300)]\ \mathrm{s}^{-1} \qquad (x \le -63) \qquad (44)$$

The value of $f'(II')$ at $x = 60$ is 140 s^{-1} (compare $f = 500\ s^{-1}$) and $f(II')$ at $x = -63$ is 88 s^{-1} (compare $f' = 4000\ s^{-1}$).

The calculation of $\bar{F}/\bar{F}_0$ for models II and II′ is shown as solid circles in Fig. 9 and as a solid curve through these points in Fig. 12. Except for a difference of 0.004 at $v = 6$ Å · ms^{-1}, the calculated values of $\bar{F}/\bar{F}_0$ for the two models differ by at most 0.002. The agreement with experiment (Fig. 9) is not good (being very similar to model I′).

Fig. 12 (solid curves) includes, in addition, the ATP flux, efficiency, and cycles per

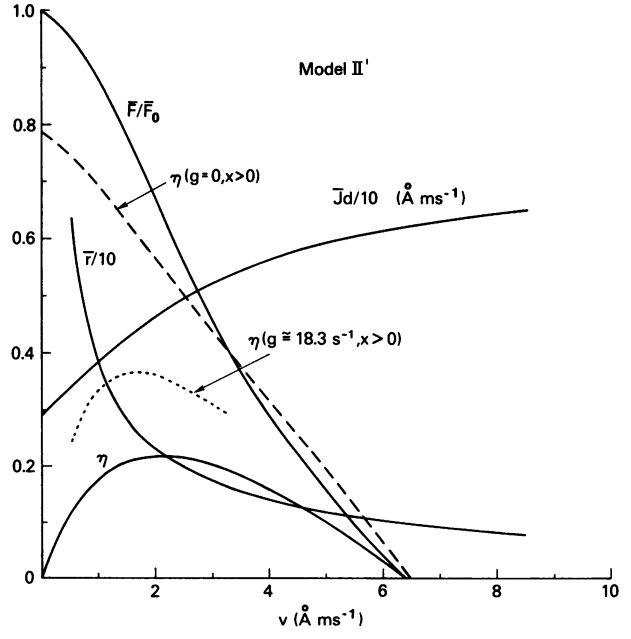

FIGURE 12 Solid curves: computed steady properties of model II′ ($g = 50\ s^{-1}$ at $x > 0$). The dashed and dotted curves show the effect on the efficiency of lowering g at $x > 0$.

pass for model II′, as functions of velocity (incidentally, the values of $\bar{J}d$ for models II and II′ differ by at most 0.02 Å · ms^{-1}). As compared with model I′ (Fig. 10), the flux is smaller and has a larger proportional increase with v. The maximum efficiency η^* is about 22% at $v^* \cong 2.2$ Å · ms^{-1}. The value of $\bar{r}$ at v^* is about 2.2.

Although the steady force-velocity curve is unsatisfactory for model II, Podolsky and Nolan (unpublished) computed and found realistic isotonic transients for this model. In view of the slight differences, already noted, between models II and II′, the transients for the two cases are presumably very similar. Consequently, we have not computed transients for model II′. The fraction of attached cross-bridges for model II′ is calculated to be $\bar{n}_0 = 0.166$ (essentially as expected from $d = 360$ Å and an f function of width 60 Å).

Change of g Value in Model II′. The discussion of the variation of g under (*b*) (model I′), above, is applicable here as well except for the following changes in numbers: $g = 50$ s^{-1} (at $x > 0$) in model II′ to begin with; $a = 63$ Å; $\bar{J}_0 d = 2.918$ Å · ms^{-1} when $g = 50$ s^{-1} ($x > 0$); and $g \cong 18.3$ s^{-1} ($x > 0$) produces (by interpolation) the experimental value of $\bar{J}_0 d$.

The dashed and dotted curves in Fig. 12 show the recalculated efficiency for $g = 0$ and $g \cong 18.3$ s^{-1}, respectively, at $x > 0$. The same values as in (*b*) are found (from the dotted curve in Fig. 12) for η^*, v^*, and $\bar{r}$ at v^*: 0.37, 1.7 Å ms^{-1}, and 1.6, respectively.

Model II′ Near Equilibrium ($\Delta \to 0$). We supplement the near-equilibrium results of Hill and Chen (1974) with the calculation of A, B, C, D from Eqs. 27–30 for this much more realistic model. We put $g^e = 10^{-8}\, g$ (that is, we use the special case $g = g^e e^{\Delta}$ referred to near the end of section 3). Extension of g to $x > 60$ (dashed line in Fig. 11), along with g' from Eq. 12, is essential. We find that $A = D$ (as a check) and that

$$\begin{aligned} Ad\sigma^2 &= 23.91 \text{ Å}^2 \\ Bd\sigma^4/kT &= 1.416 \times 10^{13} \text{ Å}^3 \cdot \text{ms} \\ CdkT &= 2.973 \times 10^{-8} \text{ Å} \cdot \text{ms}^{-1} \\ A^2/BC &= 1.358 \times 10^{-3} \\ \eta^*_{eq} &= 3.395 \times 10^{-4}. \end{aligned} \tag{45}$$

The physiological efficiency (above) is $\eta^*_p \cong 0.22$. The ratio of the two efficiencies is 6.5×10^2. In the Hill and Chen (1974) example, η^*_p was also much larger than η^*_{eq}, with a ratio 2.1×10^4.

(d) Models III and III′

Models I′ and II′ are the only modified Podolsky-Nolan models for which we have made complete calculations of steady properties. Both models give practically the same rather unsatisfactory force-velocity curve (Fig. 9). As already mentioned, we have made no attempt systematically to improve these models. However, that considerable improvement is easily possible can be seen from another unpublished model (III) of Podolsky and Nolan, which is included in Figs. 9 and 11. It will be noted in the former figure that the force-velocity relation is, on the whole, closer to the ex-

perimental points than is the case for models I′ and II′. Further, the (unpublished) isotonic transients for model III are very satisfactory. In fact, the time course of the early rapid phase of the transients for model III is closer to the experimental motion than that of models I and II.

Model III differs from model II only in the shape of the f function (Fig. 11). In view of the results found above for models II and II′, we can use the same (or, preferably, slightly adjusted) x_+ and x_- as in model II′, leave the gap as it is, and expect with confidence that model III′ will have essentially the same transient and steady properties as already computed for model III. Hence, we omit the details of model III′, and we have made no actual calculations for this model.

It seems to us probable, though this remains to be seen, that a systematic adjustment of model III′ could produce a self-consistent model with: (*a*) satisfactory transients; (*b*) satisfactory force-velocity relation; (*c*) efficiency in the 35–50% range; and (*d*) virtual elimination of physically unrealistic appendages such as $f(II')$ and $f'(II')$ (Fig. 11). Item (*d*) could be accomplished, for example, by using a steeper F_1 at negative x so that both x_- and x_+ can be moved somewhat to the right (Fig. 11).

(e) Other Models

We have also calculated steady isotonic properties for a number of self-consistent variations on Podolsky-Nolan of the sort illustrated in Fig. 13 (with analytical functions). The model in Fig. 13 illustrates, for example, how the discontinuous cut-offs used by Podolsky and Nolan might be avoided. We anticipated that the particular models of this type that we examined would have relatively poor transient properties, so they were not pursued further. For the model shown in Fig. 13, we used $F_1/K = x$ for $x \geq 0$ and $F_1/K = x - (x^2/15)$ for $x \leq 0$. Also, we took $e^{\Delta p} = 10^8$, $e^{\Gamma} = 3.704 \times 10^6$, $x_+ = 110$, $x_- \cong -58$, and $\sigma = 20$ Å. The g' function is not visible on the scale of Fig. 13. This model had an efficiency $\eta^* = 0.34$ at $v^* \cong 6.5$ Å $\cdot$ ms^{-1} (where $\bar{r} \cong 1.5$). Note the approximate inverse correlation between η^* and $\bar{r}$ (at v^*): model I′, $\eta^* = 0.12$, $\bar{r} = 3.4$; model II′, $\eta^* = 0.22$, $\bar{r} = 2.2$; this model, $\eta^* = 0.34$, $\bar{r} = 1.5$; and the reduced g models I′ and II′, $\eta^* = 0.37$, $\bar{r} = 1.6$. The idealized two-state model in the next section has $\bar{r}$ near unity and a very high efficiency.

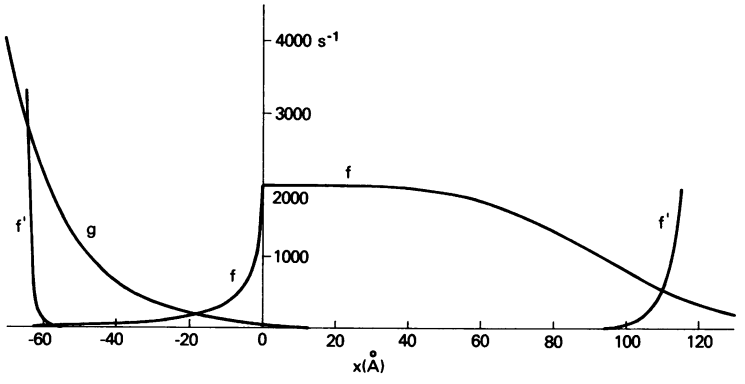

FIGURE 13 A variation on Podolsky-Nolan models. Here $F_1/K = x$ for $x > 0$ and $F_1/K = x - (x^2/15)$ for $x < 0$. The function $g'(x)$ is not visible on this scale. This model gives an efficiency $\eta^* = 0.34$.

TABLE I
COMPUTED ISOMETRIC FORCE

Model	$\bar{F}_0 d\sigma^2/kT$	$\bar{F}_0 d/kT$
	$Å^2$	
I	6735.0	—
I′	6513.3	13.65
II	1752.0	—
II′	1711.5	14.11
III	1777.8	—
III′	—	(14.3)
Fig. 13 (σ = 20 Å)	5262.3	13.16

(f) Magnitude of Isometric Force

The magnitude of the isometric force for all models studied in this section is given in Table I. The middle column is the directly computed quantity (with contributions of the form $\int x n_0 dx$, etc.), as, for example, in the Podolsky-Nolan calculations. This quantity is also equal to $\bar{F}_0 d/K$. The value of σ^2 (or K) is needed to obtain the last column, hence the calculation can be made only for the complete models I′, II′, III′, and Fig. 13 (the III′ value is an estimate). The result (Table I) is that all complete models give practically the same $\bar{F}_0 d/kT$.

Before discussing the actual magnitude of $\bar{F}_0 d/kT$, we consider the basis for the approximate uniformity of the $\bar{F}_0 d/kT$ values for the three modified Podolsky-Nolan models (I′–III′) in Table I. Let h be the width of the f function at positive x (h = 120 Å or 60 Å, Figs. 8 and 11). To a rather good approximation in these models, $n_0 = 1$ in the interval $0 \leq x \leq h$ and $n_0 = 0$ otherwise. Therefore

$$\bar{F}_0 \cong \frac{1}{d} \int_0^h (kT/\sigma^2) x \, dx = kTh^2/2d\sigma^2. \tag{46}$$

Also, the value of σ^2 is given by $\sigma^2 = x_+^2/2\Gamma$. Thus we have

$$\bar{F}_0 d/kT \cong \Gamma(h^2/x_+^2), \tag{47}$$

where h^2/x_+^2 has the value 0.937 for model I′ and 0.921 for model II′. We have used in this paper (to some extent arbitrarily) $e^\Gamma = 10^7$ or $\Gamma = 16.12$. Thus the approximate values of $\bar{F}_0 d/kT$ we find from Eq. 47 are 15.1 and 14.8, respectively. Use of the actual $n_0 < 1$ would have reduced these values slightly. It is apparent, then, that the uniformity referred to above is simply a consequence of $x_+ \cong h$ and of the same choice of Γ for all models.

Incidentally, Eq. 61 below, for a different model, is very similar to Eq. 47. The physical significance of $\bar{F}_0 d \cong \Gamma kT$ in both cases is obvious from Fig. 7*b* and Eq. 22 (with $v \to 0$): the work obtained ($\bar{F}_0 d$) in a low velocity pass is approximately equal to the full free energy drop (ΓkT).

In comparing $\bar{F}_0 d/kT \cong 14.3$ (which we take as the best Podolsky-Nolan value in Table I) with experiment, let us introduce the experimental value of $\bar{F}_0$ into this equation, calculate d, and see if it makes sense. To be reasonable, d should at least equal the "width" of the model, as measured by the range of finite $n(x)$ at v_{max}. This range is about 200 Å for model I′ and about 130 Å for models II′ and III′. The optimal value would be $d = 360$ Å (actin repeat).

To estimate $\bar{F}_0$, we begin with a myosin filament of length 1.6 μm, a bare region of length 0.16 μm, a repeat distance of 430 Å (Squire, 1973), and we assume 12 myosin molecules per repeat (Morimoto and Harrington, 1974). There are then 200 myosin molecules per half-filament. At rest length, we take the nearest-neighbor distance in the hexagonal array of myosin filaments to be 412 Å (Huxley and Brown, 1967). The number of myosin molecules $\cdot$ mm^{-2} per half-sarcomere is then 1.36×10^{11}. If we use for the maximum observed isometric tension (at 3°C) a value 3.0×10^4 dyn mm^{-2} (Gordon et al., 1966), we find $\bar{F}_0 = 2.21 \times 10^{-7}$ dyn for the isometric force per overlap cross-bridge. Then $\bar{F}_0 d/kT = 14.3$ leads to $d \cong 250$ Å, which is "reasonable" but not "optimal" (see above). Since in this calculation the value found for d is proportional to the value used for Γ (Eq. 47), we note that if we had taken $e^{\Gamma} = 10^9$, as suggested in section 4 (*b*) above, we would have found $d \cong 320$ Å.

Magnitude of K. We have already encountered values for K, at 3°C, of 0.80 erg $\cdot$ cm^{-2} (model I′) and 3.14 erg $\cdot$ cm^{-2} (model II′). These are direct consequences of our choices of x_+ and Γ (Eq. 36). If we had used $e^{\Gamma} = 10^9$ instead of 10^7, we would have obtained $K = 1.03$ erg $\cdot$ cm^{-2} (model I′) and 4.04 erg $\cdot$ cm^{-2} (model II′).

The experimental instantaneous stiffness together with the theoretical values of $\bar{n}_0$ (the fraction of attached cross-bridges) for models I′ and II′, above, furnish independent estimates of K for comparison with the values above. For purposes of this calculation, we have to assume that there is no passive series elasticity. The simplest theoretical relation (which is all we use) between the instantaneous force per cross-bridge, $\bar{F}(0;y)$, and $\bar{F}_0$ is (Hill, 1974, Eq. 44)

$$\bar{F}(0;y) = \bar{F}_0 + \bar{n}_0 K y,$$

where y is the instantaneous change in length per half-sarcomere. Ford et al. (1974) have found that $\bar{F}(0;y) = 0$ when $y \cong -50$ Å. Using $\bar{F}_0 = 2.21 \times 10^{-7}$ dyn from above, we then deduce that $\bar{n}_0 K = 0.442$. To find K itself we also need $\bar{n}_0$. On introducing $\bar{n}_0 = 0.32$ (model I′) and $\bar{n}_0 = 0.166$ (model II′), we obtain finally $K = 1.38$ erg $\cdot$ cm^{-2} (model I′) and $K = 2.66$ erg $\cdot$ cm^{-2} (model II′). The K values from the two sources (x_+ and Γ; stiffness) agree as to order of magnitude.

5. IDEALIZED TWO-STATE HIGH-EFFICIENCY MODEL

The two-state model considered here is perhaps as simple a self-consistent model as can be constructed. It represents a kind of asymptotic limit in two-state model construction; it is therefore very unreal. But it is of interest because it demonstrates the possibility of very high efficiencies, and at the same time might provide an upper limit in this

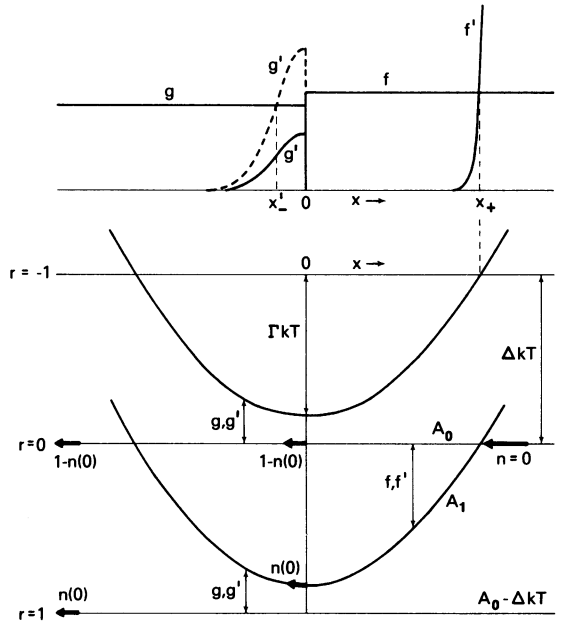

FIGURE 14 *Top:* rate constant functions for the idealized model of section 5 in the case $\Delta > \Gamma$ (the dashed g' curve illustrates $\Gamma > \Delta$); f and f' are zero at negative x while g and g' are zero at positive x. *Bottom:* corresponding free energy curves with possible transitions indicated by double arrows, for the pass of an actin site starting on the right at the $r = 0$ level. Heavy arrows indicate schematically the fate of the initial unit probability packet labeled $n = 0$.

respect for two-state models. Of course in "real" two-state models (e.g. section 4), one must make a sacrifice with regards efficiency for the sake of adequate mechanical and other properties.

As shown in Fig. 14 (see also Fig. 3), f is constant for $x \geq 0$ and $f = 0$ for $x < 0$. Conversely, g is constant for $x < 0$ and $g = 0$ for $x \geq 0$. The ratio g/f is arbitrary. The force and free energy functions for the attached state are taken as

$$\begin{aligned} F_1 &= Kx = (kT/\sigma^2)x \\ A_1 &= A_1^0 + \frac{1}{2}Kx^2. \end{aligned} \tag{48}$$

It then follows from Eqs. 11 and 12 that (Fig. 14)

$$\begin{aligned} f'/f &= e^{-\Gamma}e^{x^2/2\sigma^2} \qquad (x \geq 0) \\ &= 0 \qquad\qquad\quad (x < 0) \end{aligned} \tag{49}$$

and

$$\begin{aligned} g'/f &= (g/f)e^{\Gamma-\Delta}e^{-x^2/2\sigma^2} \qquad (x < 0) \\ &= 0 \qquad\qquad\qquad\quad (x \geq 0), \end{aligned} \tag{50}$$

where the constant f is used as a reference rate constant. The magnitude of g' relative to g (Figs. 6 *d* and 6 *e*) depends on $\Gamma - \Delta$. Fig. 14 is drawn for the case $\Delta > \Gamma$ (except for the dashed g' curve, which corresponds to $\Gamma > \Delta$). In the numerical calculations described below (steady isotonic contractions) we take $e^{\Delta} = 10^8$ = constant and vary (somewhat) the remaining independent parameters e^{Γ}, g/f, and $v/\sigma f$.

The essence of the model is that at positive x only f, f' transitions occur while at negative x only g, g' transitions occur. From a stochastic point of view, in the pass of an actin site by a cross-bridge, the site approaches the cross-bridge from positive x (heavy arrow on right, Fig. 14) certainly unattached ($n = 0$). Only f, f' transitions (double arrow) are possible, and these strongly favor attachment, until $x = 0$ is reached, at which point $n = n(0)$. The two probability packets, $1 - n(0)$, unattached, and $n(0)$, attached (smaller heavy arrows), both then may undergo g, g' transitions but the packets must eventually end up intact, despite these transitions, with the same values $1 - n(0)$ and $n(0)$, respectively, at large negative x (Fig. 14). However, the state of the packet $n(0)$ switches from attached (state 1) at $x = 0$ to unattached (state 0) at $x = -\infty$. That is, there is a net g, g' flux in this interval, proportional to $n(0)$. Obviously, $\bar{r} = n(0) \leq 1$ since there is no way r (at the end of a pass) can have any value (e.g., -1, $+2$) other than $r = 0$ and $r = 1$. Since $\bar{J} = \bar{r}v/d$ in general, we must have here $\bar{J} = n(0)v/d$ (as, in fact, is self-evident). Of course $n(0)$ itself depends on v. Note that $\bar{J} \to 0$ as $v \to 0$. This, too, is obvious from the model since f and f' do not overlap with g and g' in any interval of x.

The approximate efficiency in the limit of low velocities ($v \to 0$) can be deduced, by inspection, for the two special cases shown in Fig. 15. The isometric steady state, at

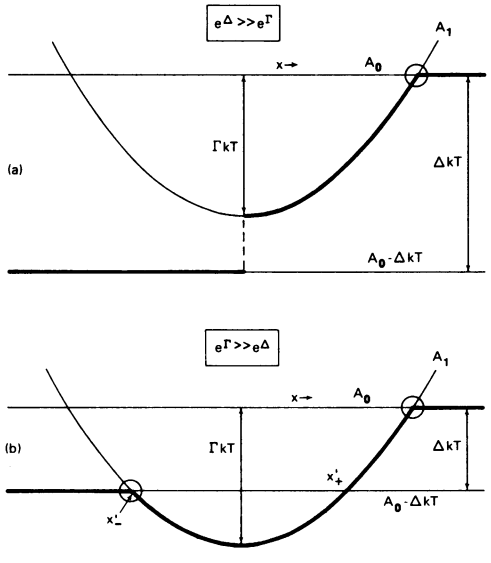

FIGURE 15 Section 5 model: basis of approximations, for low velocity ($v \to 0$) contractions, that (*a*) $\eta \cong \Gamma/\Delta$ for $e^{\Delta} \gg e^{\Gamma}$ and (*b*) $\eta \cong 1$ for $e^{\Gamma} \gg e^{\Delta}$. See text for details.

positive x, amounts to f, f' equilibrium between free energy levels A_0 and A_1 (highly favoring A_1) and at negative x, to g,g' equilibrium between free energy levels A_1 and $A_0 - \Delta kT$ (see Eqs. 11 and 12). The heavy lines in Fig. 15 show the highly favored free energy level for each x. The circles indicate schematically the regions where the "highly favored" simplification is inaccurate. It is apparent from the heavy lines that, for very low velocity passes, the efficiency will be $\eta \cong \Gamma/\Delta$ for the case $e^{\Delta} \gg e^{\Gamma}$ (compare Fig. 7 *b*) and $\eta \cong 1$ for the case $e^{\Gamma} \gg e^{\Delta}$ (negative and positive contributions to the work, from $x'_- \leq x \leq x'_+$, cancel). These estimates will be confirmed below.

We turn now to a more systematic analysis. The differential equations, in dimensionless form, are

$$-\left(\frac{v}{\sigma f}\right)\frac{dn}{d(x/\sigma)} = 1 - n - (f'/f)n \qquad (x \geq 0) \tag{51}$$

$$= (g'/f)(1 - n) - (g/f)n \qquad (x < 0). \tag{52}$$

The boundary condition on Eq. 51 is $n = 0$ at $x = \infty$; on Eq. 52, it is $n = n(0)$, obtained from the solution of Eq. 51, at $x = 0$. Because of the presence of f'/f and g'/f, the solutions of these equations for arbitrary $v/\sigma f$ cannot be expressed in terms of elementary functions. Of course $n(-\infty) = 0$. The isometric ($v = 0$) solutions are

$$n_0(x) = f/(f + f') = e^{\Gamma}/(e^{\Gamma} + e^{x^2/2\sigma^2}) \qquad (x \geq 0) \tag{53}$$

$$= g'/(g + g') = e^{\Gamma-\Delta}/(e^{\Gamma-\Delta} + e^{x^2/2\sigma^2}) \qquad (x < 0). \tag{54}$$

Substitution of either Eq. 51 or 52 into the integrand of Eq. 20 for $\bar{J}$ allows immediate integration of $\int dn$ over $0 \leq x \leq \infty$ or $-\infty \leq x \leq 0$, respectively, with the result

$$\bar{J}d/\sigma f = (v/\sigma f)n(0), \tag{55}$$

as already deduced above by another argument. The quantities $n(0)$ and $\bar{J}d/\sigma f$ depend on Eq. 51 but not on Eq. 52. Therefore, they are functions of e^{Γ} and $v/\sigma f$ but not of e^{Δ} or g/f.

When e^{Γ} is large (say, $\geq 10^6$), as in practical examples, a good approximation to $n(0)$ can be obtained by omitting f' and, as compensation, giving f a step down to zero at $x = x_+ = \sigma(2\Gamma)^{1/2}$ (Fig. 14). Integration of Eq. 51, with $n = 0$ at $x = x_+$, then gives

$$n(x) \cong 1 - \exp[-(2\Gamma)^{1/2}/(v/\sigma f)]\exp(xf/v) \qquad (0 \leq x \leq x_+). \tag{56}$$

We can see from this approximation that, for $v/\sigma f$ of order unity or less, $n(0) \cong 1$ and $\bar{J}d/\sigma f \cong v/\sigma f$. Exact computer solution of Eq. 51, for $n(0)$, gives $\bar{J}d/\sigma f = 0.5000$ for $v/\sigma f = 0.5$ and $e^{\Gamma} = 10^7, 10^8, 10^9$, and $\bar{J}d/\sigma f = 0.9971, 0.9980, 0.9986$ for $v/\sigma f = 1.0$ and the same values of e^{Γ}, respectively.

The force (Eq. 19) cannot be expressed simply except in the isometric case:

TABLE II

COMPUTED FORCE, $\bar{F}d/kT(e^{\Delta} = 10^8)$

		$v/\sigma f = 0$	0.5	1.0
$e^{\Gamma} = 10^7, g/f =$	1	16.02	14.04	11.55
10^8	1	17.73	15.41	12.64
10^9	1	18.33	15.47	12.07
10^7	4	16.02	14.29	12.48
10^7	1	16.02	14.04	11.55
10^7	1/4	16.02	10.31	−2.76

$$\bar{F}_0 d/kT = \ln\left[\frac{e^{\Delta}(1 + e^{\Gamma})}{e^{\Delta} + e^{\Gamma}}\right] \tag{57}$$

$$\rightarrow \frac{\Delta e^{\Gamma}}{1 + e^{\Gamma}} = \Delta n_0(0) \qquad (\Delta \rightarrow 0) \tag{58}$$

$$\cong \Delta \qquad (e^{\Gamma} \gg e^{\Delta} \geq 1) \tag{59}$$

$$\cong \Delta - \ln 2 \qquad (e^{\Gamma} = e^{\Delta} \gg 1) \tag{60}$$

$$\cong \Gamma \qquad (e^{\Delta} \gg e^{\Gamma} \gg 1). \tag{61}$$

Table II contains a few computed values of the force, from Eqs. 19, 51, 52, and 57.

In Eq. 58 and below, when we let $\Delta \rightarrow 0$ (approach to equilibrium), we hold Γ constant. This amounts to adopting the special case Eq. 14*a*.

The efficiency is

$$\eta = \bar{F}v/\bar{J}\Delta kT = (\bar{F}d/kT)/n(0)\Delta. \tag{62}$$

It can be shown analytically (and is confirmed by Eq. 56 and Table II) that, for any Δ, $n(0)$ has zero slope while $\bar{F}d/kT$ has a finite negative slope, as functions of $v/\sigma f$, in the limit $v/\sigma f \rightarrow 0$. Hence, for given Δ, η in Eq. 62 has a maximum at $v = 0$: $\eta^* = \eta_0$ (isometric) and $v^* = 0$. The explicit expression for η^* is

$$\eta^* = \eta_0 = \frac{(\bar{F}_0 d/kT)}{n_0(0)\Delta} = \left(\frac{1 + e^{\Gamma}}{\Delta e^{\Gamma}}\right) \ln\left[\frac{e^{\Delta}(1 + e^{\Gamma})}{e^{\Delta} + e^{\Gamma}}\right] \tag{63}$$

$$\rightarrow 1 = \eta^*_{eq} \qquad (\Delta \rightarrow 0) \tag{64}$$

$$\cong 1 - (e^{\Delta}/\Delta e^{\Gamma}) \qquad (e^{\Gamma} \gg e^{\Delta} \geq 1) \tag{65}$$

$$\cong 1 - (\ln 2/\Delta) \qquad (e^{\Gamma} = e^{\Delta} \gg 1) \tag{66}$$

$$\cong \Gamma/\Delta \qquad (e^{\Delta} \gg e^{\Gamma} \gg 1). \tag{67}$$

Eqs. 65 and 67 confirm the estimates made above on the basis of Fig. 15. Some exact values of η are given in Table III; they range between 0.5 and 1.0.

TABLE III

COMPUTED EFFICIENCY, $\eta\,(e^{\Delta} = 10^8)$

		$v/\sigma f = 0$	0.5	1.0
$e^{\Gamma} = 10^7$,	$g/f = 1$	0.870	0.762	0.629
10^8	1	0.962	0.836	0.688
10^9	1	0.995	0.840	0.656
10^7	4	0.870	0.776	0.680
10^7	1	0.870	0.762	0.629
10^7	1/4	0.870	0.560	—

The rate of entropy production is

$$T\dot{S}_i = \bar{J}\Delta kT - \bar{F}v. \tag{68}$$

It is interesting that, in the isometric state (Δ arbitrary), $T\dot{S}_i = 0$. This result is ordinarily expected only at equilibrium. The reason it is encountered here is that we have a quasi-equilibrium when $v = 0$: at positive x, there is an f, f' equilibrium between states 0 and 1; and at negative x, there is a g, g' equilibrium between these states (see Eqs. 53 and 54). Correspondingly, the flux is zero at $v = 0$.

Eqs. 23 and 27–30 apply near equilibrium (Γ constant, $\Delta \to 0$). From Eqs. 23 and 58 we find $Ad = n_0(0)$, and this can be confirmed by use of Eq. 27. From Eqs. 23 and 55, we have $C = 0$ and $Dd = n_0(0)$. Eqs. 29 and 30 verify these latter results. The reciprocal relation, $A = D$, is satisfied. B must be computed numerically.

The efficiency, near equilibrium, is

$$\eta = \bar{F}v/\bar{J}\Delta kT = 1 - [Bdv/n_0(0)\Delta kT]. \tag{69}$$

The maximum η, for given (small) Δ, occurs at $v = 0$: $v^* = 0$, $\eta^*_{eq} = 1$, in agreement with Eq. 64. This can also be seen from Eq. 31 since $C = 0$ and $A^2/BC = \infty$.

The entropy production, near equilibrium, is $T\dot{S}_i = Bv^2$.

Approximations. For order of magnitude purposes, one can easily obtain approximate expressions for $\bar{F}$ and $\bar{J}$ in the special cases (*a*) $e^{\Delta} \gg e^{\Gamma} \gg 1$ and (*b*) $e^{\Gamma} \gg e^{\Delta} \geq 1$. In both of these cases, since $e^{\Gamma} \gg 1$, we omit f' and cut f off at $x = x_+$ (see above). Then solution of Eq. 51 gives Eq. 56 as an approximation to $n(x)$ for $0 \leq x \leq x_+$. Also, $n(x) = 0$ for $x > x_+$. Then from Eq. 55 our approximation to $\bar{J}$, in both cases, is

$$(a) \text{ and } (b): \ \bar{J}d/\sigma f \cong (v/\sigma f)\{1 - \exp[-(2\Gamma)^{1/2}/(v/\sigma f)]\}. \tag{70}$$

In case (*a*), at negative x, we omit g' since $g \gg g'$ even at $x = 0$. Eq. 52 then gives

$$(a) \quad n(x) \cong n(0)e^{gx/v} \qquad (x < 0) \tag{71}$$

where $n(0) = \{\ \}$ in Eq. 70. Eqs. 56 and 71, when substituted into Eq. 19, lead to

$$(a) \quad \bar{F}d/kT \cong \Gamma - (v/\sigma f)(2\Gamma)^{1/2} + (v/\sigma f)^2 n(0)[1 - (g/f)^{-2}]. \tag{72}$$

In case (*b*), at negative x, we assume that $n(x)$ has the constant value $n(0)$ in the interval $x'_- \leq x \leq 0$ (since $g' \gg g$), and that g' may be neglected for $x < x'_-$ (since $g \gg g'$). Thus

$$(b) \quad n(x) \cong n(0)\, e^{-gx'_-/v} e^{gx/v} \qquad (x < x'_-) \tag{73}$$

where

$$x'_- = -\sigma[2(\Gamma - \Delta)]^{1/2}. \tag{74}$$

Using the various parts of $n(x)$, we find from Eq. 19 that

$$\begin{aligned}(b) \quad \bar{F}d/kT \cong\ & n(0)\Delta + [1 - n(0)]\Gamma - (v/\sigma f)\{(2\Gamma)^{1/2} \\ & + n(0)[2(\Gamma - \Delta)]^{1/2}(g/f)^{-1}\} \\ & + (v/\sigma f)^2 n(0)[1 - (g/f)^{-2}].\end{aligned} \tag{75}$$

Introduction of a Podolsky-Nolan Gap. Suppose that the g, g' functions in Fig. 14 are interrupted at $x = -a < 0$ and replaced by f, f' functions for $x < -a$, as in Figs. 8 and 11. This generalization is very close to the reduced g models discussed in sections 4(*b*) and 4(*c*). In fact, the dashed curves in Figs. 10 and 12 are essentially (but not exactly) examples. The model shown in Fig. 14, as it stands, is the case $a \to \infty$. The physical significance of the change (finite a) is: (*1*) cross-bridges that are still attached at $x = -a$, in isotonic contractions of sufficient velocity, will now be detached via f' rather than via g (thus reducing $\bar{J}$); and (*2*) new attachments at $x < -a$, reducing the mean force, may be formed via f if v is small and if $-a$ is not much less than x_-, or especially if $-a > x_-$.

We mention only a few properties of this system, which we have not investigated thoroughly. Consideration of the revised Fig. 14 shows that now it is possible to have $r = -1$ as well as $r = 0$ and $r = +1$, at the end of a pass. Integration of Eq. 52 from $x = -a$ to $x = 0$ gives, for any v,

$$\bar{J}d = [n(0) - n(-a)]v, \quad \bar{r} = n(\tilde{0}) - n(-a) \leq 1. \tag{76}$$

Thus the isometric flux is zero. The maximum efficiency is presumably at $v = 0$ (as in the dashed curves of Figs. 10 and 12); there is quasi-equilibrium at $v = 0$ with $T\dot{S}_i = 0$; and $\eta^* = \eta_0 \to 1$ as $\Delta \to 0$. These qualitative properties are all unchanged from the $a = \infty$ case.

The isometric force is found to be

$$\frac{\bar{F}_0 d}{kT} = \ln\left[\frac{(e^{\Gamma-\Delta} + e^z)(e^\Gamma + 1)}{(e^{\Gamma-\Delta} + 1)(e^\Gamma + e^z)}\right], \tag{77}$$

where $z = a^2/2\sigma^2$, while

$$n_0(0) - n_0(-a) = [e^\Gamma/(e^\Gamma + 1)] - [e^{\Gamma-\Delta}/(e^{\Gamma-\Delta} + e^z)]. \tag{78}$$

The isometric efficiency, η_0, follows from Eqs. 77 and 78. One can show that η_0 as a function of

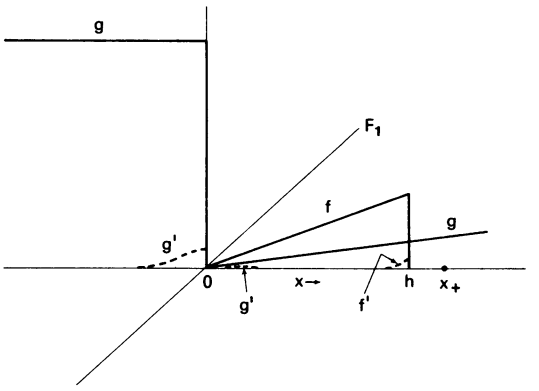

FIGURE 16 A. F. Huxley (1957) model with minor (or negligible) additions (dashed curves) needed for completeness, along with Γ and Δ values.

a (Δ and Γ constant) has a maximum at $a \rightarrow \infty$. Introduction of f, f' for $x < -a$ lowers $\bar{F}_0$ more than it lowers $n_0(0) - n_0(-a)$; hence $\eta^* = \eta_0$ is larger in the original model ($a = \infty$) than in the modified model (a finite).

Note that, because of the quasi-equilibrium at $v = 0$, the above *isometric* properties do not depend at all on the shapes of f, f', g, g' but only on the values of Γ, Δ, and z.

A. F. Huxley (1957) Model. The original A. F. Huxley (1957) model resembles the present one to some extent. For the Huxley model to be "legal" (Fig. 16) as it stands requires: (*1*) location of $x_+ = \sigma(2\Gamma)^{1/2}$ sufficiently to the right of $x = h$ so that the f' appendage (dashed) will be negligible; and (*2*) $e^{\Delta} \gg e^{\Gamma}$ so that the g' appendages (dashed) will also be negligible. The latter condition would limit the possible efficiency (compare Fig. 7*b* and Eq. 67). Thus, to complete the model, Γ and Δ need specification (Huxley includes K and d in his equations).

APPENDIX

This appendix is concerned with the form of the dependence of certain rate constants on the concentrations of ATP, ADP, and P. Actually, except for some incidental calculations near equilibrium, this question does not arise in sections 4 and 5 because these concentrations are held constant. But in other experimental and theoretical work, this subject could be of importance.

If we deal with a complete diagram that uses elementary molecular transitions, the situation is simple (Hill, 1974, 1975*a*). If $\lambda = e^{\mu/kT}$ is the absolute activity of any ligand (ATP, ADP, P), the first-order rate constant for binding the ligand is proportional to λ and the inverse (desorption) rate constant is independent of λ. Of course, λ is proportional to concentration c if the activity coefficient can be ignored. We use $\lambda \sim c$ below.

The above simple relationships can become more complicated if elementary transitions are not used, that is, if the complete diagram is compressed or reduced to a smaller number of states (Hill, 1975*a*, Appendix 2). Such complications are especially to be expected in the most extreme case of diagram compression or reduction, namely, to two states (as in the present paper).

We confine our comments below to biochemical diagrams in which no cycle of the diagram involves the splitting of more than one ATP molecule per single circuit around the cycle.

Single Cycle

We consider first the most important special case (in the present state of the subject): only one cycle of the complete diagram is important. Thus we are concerned here with the reduction of a single cycle to, possibly, as few as two states.

Let $\alpha_T \sim \lambda_T$ (or c_T) be the elementary first-order binding rate constant for T and let β_T be the corresponding desorption rate constant (and similarly for D). Then if a sequence (counterclockwise in Fig. 1) of two or more successive inverse pairs of transitions in the cycle, including the pair α_T, β_T but not including α_D, β_D, are reduced to a single pair of effective transitions (Hill, 1975*a*, Appendix 2), the effective first-order rate constants will have a dependence on c_T of the form

$$\alpha_T^* = [\alpha_T^{*e}(1 + a)(c_T/c_T^e)]/[1 + a(c_T/c_T^e)] \tag{79}$$

$$\beta_T^* = [\beta_T^{*e}(1 + a)]/[1 + a(c_T/c_T^e)], \tag{80}$$

where a is a positive quantity (or zero) that depends on the particular case. Eq. 79 has the form of a Langmuir adsorption isotherm. Similarly, for a sequence (in the opposite direction) that includes the pair α_D, β_D but not α_T, β_T, we have

$$\alpha_D^* = [\alpha_D^{*e}(1 + b)(c_D/c_D^e)]/[1 + b(c_D/c_D^e)] \tag{81}$$

$$\beta_D^* = [\beta_D^{*e}(1 + b)]/[1 + b(c_D/c_D^e)], \tag{82}$$

where $b \geq 0$.

Actually, a and b are constant with respect to variations in c_T and c_D, but in general they are both functions of x (since they involve combinations of more elementary rate constants), as are also α_T^{*e}, etc. This feature makes the application of Eqs. 79–82 to a particular model rather awkward except in the special cases $a, b \to 0$, $a, b \gg 1$, or a, b independent of x.

If the above kind of reduction of a single cycle is carried out all the way to two states, and if we assign g, g' to the T transitions and f, f' to the D transitions (this is the case in Eq. 14*b*), then we have, above,

$$g = \alpha_T^*, g' = \beta_T^*, f' = \alpha_D^*, f = \beta_D^*. \tag{83}$$

If we put $c_D/c_D^e \equiv 1$ (i.e., c_D is not varied) and $a = 0$, so that $g = g^e(c_T/c_T^e) = g^e e^{\Delta}$ and $g' = g'^e$, we have the simple special case used in most of our previous work.

Eqs. 79–82 provide an illustration of Eqs. 24. One finds that

$$\begin{aligned} a_1 &= -\frac{b}{1+b}\frac{(\Delta c_D/c_D^e)}{\Delta}, \quad a_2 = \frac{1}{1+b}\frac{(\Delta c_D/c_D^e)}{\Delta} \\ a_3 &= \frac{1}{1+a}\frac{(\Delta c_T/c_T^e)}{\Delta}, \quad a_4 = -\frac{a}{1+a}\frac{(\Delta c_T/c_T^e)}{\Delta}, \end{aligned} \tag{84}$$

where $\Delta c_D \equiv c_D - c_D^e$, etc., and

$$\Delta = (\Delta c_T/c_T^e) - (\Delta c_D/c_D^e).$$

It would also be possible in the reduction of a sequence of pairs of transitions to include *both* of the pairs α_T, β_T and (with opposite "polarity") α_D, β_D. We could then have effective rate constants of the form

$$\alpha^* = \frac{\alpha^{*e}(1 + a' + b')(c_T/c_T^e)}{1 + a'(c_T/c_T^e) + b'(c_D/c_D^e)} \tag{85}$$

$$\beta^* = \frac{\beta^{*e}(1 + a' + b')(c_D/c_D^e)}{1 + a'(c_T/c_T^e) + b'(c_D/c_D^e)} . \tag{86}$$

These resemble two-component Langmuir equations. If the reduction leaves only two states, there are two possibilities (as in Eqs. 14 *a* and 14 *c*):

$$\begin{aligned} &(a) \quad g = \alpha^*, g' = \beta^*; f, f' = \text{independent of } c_T, c_D \\ &(c) \quad f = \alpha^*, f' = \beta^*; g, g' = \text{independent of } c_T, c_D. \end{aligned} \tag{87}$$

In (*a*), the simple case $g = g^e e^{\Delta}$ is again obtained if $c_D/c_D^e \equiv 1$ and $a' = 0$.

Multicycled Diagram

With more than one important cycle in a diagram, it is possible to get dependences on c_T and c_D of higher order than the quotients of linear expressions encountered in the preceding subsection. For example, if there are two different paths, in a diagram, from state i to state j and each path has a reduced first-order rate constant of the form of Eq. 79, then the single effective rate constant for $i \rightarrow j$ is the sum of the two linear quotients. But this is equivalent to a quotient of two quadratic expressions.

The order becomes quartic for $i \rightarrow k$ if $i \rightarrow j$, involving c_T, is arranged in series with a similar diagram loop $j \rightarrow k$, involving c_D (opposite polarity), where j is now also a transient intermediate.

The discussion in this appendix is not exhaustive. But it should suffice to show that the possible dependences of *individual* rate constants on c_T and c_D can be various and sometimes complicated.

We are grateful to Dr. A. C. Nolan for helpful discussions.

Received for publication 11 October 1974.

REFERENCES

BAGSHAW, C. R., J. F. ECCLESTON, F. ECKSTEIN, R. S. GOODY, H. GUTFREUND, and D. R. TRENTHAM. 1974. The magnesium ion-dependent adenosine triphosphatase of myosin. Two-step processes of adenosine triphosphate association and adenosine diphosphate dissociation. *Biochem. J.* **141**:351.

CARLSON, F. D., and D. R. WILKIE. 1974. Muscle Physiology. Prentice-Hall, Inc., Englewood Cliffs, N. J.

CHEN, Y., and T. L. HILL. 1974. Analysis of a simple prototypal muscle model near to and far from equilibrium. *Proc. Natl. Acad. Sci. U.S.A.* **71**:1982.

CIVAN, M. M., and R. J. PODOLSKY. 1966. Contraction kinetics of striated muscle fibres following quick changes in load. *J. Physiol.* **184**:511.

CURTIN, N. A., C. GILBERT, K. M. KRETZSCHMAR, and D. R. WILKIE. 1974. The effect of the performance of work on total energy output and metabolism during muscular contraction. *J. Physiol.* **238**:455.

EISENBERG, E., and W. W. KIELLEY. 1973. Evidence for a refractory state of heavy meromyosin and sub-

fragment-1 unable to bind to actin in the presence of ATP. *Cold Spring Harbor Symp. Quant. Biol.* **37:** 145.

FORD, L. E., A. F. HUXLEY, and R. M. SIMMONS. 1974. Mechanism of early tension recovery after a quick release in tetanized muscle fibres. *J. Physiol.* **240**:42P.

GORDON, A. M., A. F. HUXLEY, and F. J. JULIAN. 1966. The variation in isometric tension with sarcomere length in vertebrate muscle fibres. *J. Physiol.* **184**:170.

HILL, T. L. 1968 *a*. On the sliding-filament model of muscular contraction, II. *Proc. Natl. Acad. Sci. U.S.A.* **61**:98.

HILL, T. L. 1968 *b*. Thermodynamics for Chemists and Biologists. Addison-Wesley Publishing Co., Reading, Mass.

HILL, T. L. 1973. Theory of muscular contraction extended to groups of actin sites. *Proc. Natl. Acad. Sci. U.S.A.* **70**:2732.

HILL, T. L. 1974. Theoretical formalism for the sliding filament model of contraction of striated muscle, Part I. *Prog. Biophys. Mol. Biol.* **28**:267.

HILL, T. L. 1975 *a*. Theoretical formalism for the sliding filament model of contraction of striated muscle, Part II. *Prog. Biophys. Mol. Biol.* **29.** In press.

HILL, T. L. 1975 *b*. Free energy and the kinetics of biochemical diagrams, including active transport. *Biochemistry.* In press.

HILL, T. L., and Y. CHEN. 1974. Further analysis of a simple prototypal muscle model near to and far from equilibrium. *Proc. Natl. Acad. Sci. U.S.A.* **71**:2478.

HUXLEY, A. F. 1957. Muscle structure and theories of contraction. *Prog. Biophys. Mol. Biol.* **7**:255.

HUXLEY, H. E. 1969. The mechanism of muscular contraction. *Science (Wash. D. C.).* **164**:1356.

HUXLEY, H. E., and W. BROWN. 1967. The low-angle X-ray diagram of vertebrate striated muscle and its behaviour during contraction and rigor. *J. Mol. Biol.* **30**:383.

KUSHMERICK, M. J., and R. E. DAVIES. 1969. The chemical energetics of muscle contraction. II. The chemistry, efficiency and power of maximally working sartorius muscles. *Proc. R. Soc. Lond. B Biol. Sci.* **174:** 315.

LYMN, R. W., and E. W. TAYLOR. 1971. Mechanism of adenosine triphosphate hydrolysis by actomyosin. *Biochemistry.* **10**:4617.

MORIMOTO, K., and W. F. HARRINGTON. 1974. Substructure of the thick filament of vertebrate striated muscle. *J. Mol. Biol.* **83**:83.

MULIERI, L. A., B. S. MULIERI, and K. A. P. EDMAN. 1974. Force-velocity relation in single muscle fibers. *Fed. Proc.* **33**:383.

PODOLSKY, R. J., and C. NOLAN. 1971. *In* Contractility of Muscle Cells and Related Processes. R. J. Podolsky, editor. Prentice-Hall, Inc., Englewood Cliffs, N. J.

PODOLSKY, R. J., and C. NOLAN. 1973. Muscle contraction transients, cross-bridge kinetics, and the Fenn effect. *Cold Spring Harbor Symp. Quant. Biol.* **37**:661.

PODOLSKY, R. J., A. C. NOLAN, and S. A. ZAVELER. 1969. Cross-bridge properties derived from muscle isotonic velocity transients. *Proc. Natl. Acad. Sci. U.S.A.* **64**:504.

SQUIRE, J. M. 1973. General model of myosin filament structure III. Molecular packing arrangements in myosin filaments. *J. Mol. Biol.* **77**:291.